27-Hydroxycholesterol impairs neuronal glucose uptake through an IRAP/GLUT4 system dysregulation

Muhammad-Al-Mustafa Ismail,[1]* Laura Mateos,[1]* Silvia Maioli,[1] Paula Merino-Serrais,[1] Zeina Ali,[4] Maria Lodeiro,[1] Eric Westman,[2] Eran Leitersdorf,[6] Balázs Gulyás,[3] Lars Olof-Wahlund,[2] Bengt Winblad,[1] Irina Savitcheva,[5] Ingemar Björkhem,[4] and Angel Cedazo-Mínguez[1]

[1]Division of Neurogeriatrics and [2]Division of Clinical Geriatrics, Center for Alzheimer Research, Department of Neurobiology, Care Sciences, and Society, Karolinska Institutet, 141 86 Stockholm, Sweden
[3]Centre for Psychiatry Research, Department of Clinical Neuroscience, Karolinska Institutet, 171 77 Stockholm, Sweden
[4]Division of Clinical Chemistry, Department of Laboratory Medicine and [5]Department of Radiology, Karolinska University Hospital, 141 86 Huddinge, Sweden
[6]Center for Research, Prevention, and Treatment of Atherosclerosis, Hadassah Hebrew University Medical Center, Jerusalem 91120, Israel

Hypercholesterolemia is associated with cognitively deteriorated states. Here, we show that excess 27-hydroxycholesterol (27-OH), a cholesterol metabolite passing from the circulation into the brain, reduced in vivo brain glucose uptake, GLUT4 expression, and spatial memory. Furthermore, patients exhibiting higher 27-OH levels had reduced ^{18}F-fluorodeoxyglucose uptake. This interplay between 27-OH and glucose uptake revealed the engagement of the insulin-regulated aminopeptidase (IRAP). 27-OH increased the levels and activity of IRAP, countered the IRAP antagonist angiotensin IV (AngIV)–mediated glucose uptake, and enhanced the levels of the AngIV-degrading enzyme aminopeptidase N (AP-N). These effects were mediated by liver X receptors. Our results reveal a molecular link between cholesterol, brain glucose, and the brain renin-angiotensin system, all of which are affected in some neurodegenerative diseases. Thus, reducing 27-OH levels or inhibiting AP-N maybe a useful strategy in the prevention of the altered glucose metabolism and memory decline in these disorders.

INTRODUCTION

Brain glucose metabolism is tightly regulated, and its disruption is an important feature of neurodegenerative disorders. Hypometabolism of glucose is observed in healthy older individuals (Wirth et al., 2013) and several other progressive neurodegenerative disorders exhibiting cognitive decline (Teune et al., 2010). In Alzheimer's disease (AD), glucose hypometabolism precedes the onset of memory deficits and is speculated to be a predictor of disease progression (Nordberg et al., 2010).

Few clinical studies have highlighted the importance of serum cholesterol in brain glucose uptake. Reiman et al. (2010) reported that higher serum total cholesterol levels are associated in humans with lower cerebral metabolic glucose rate in areas affected in AD, but also in other areas commonly affected by normal aging. In animal models for AD and aging, cognitive decline was evident when subjected to a high-cholesterol diet (HCD; Pancani et al., 2013; Knight et al., 2014). Hypercholesterolemia confers a higher risk for AD (Kivipelto et al., 2001), and emerging evidence suggests that disruption of cholesterol metabolism plays a pivotal role in cognitive deficits associated with other neurodegenerative disorders (Hottman et al., 2014).

Unlike cholesterol, its side-chain oxidized form, known as oxysterol, can traverse the blood–brain barrier from both directions (Björkhem et al., 2009). Higher levels of 27-hydroxycholesterol (27-OH) were found in brains and cerebrospinal fluid (CSF) from AD patients (Heverin et al., 2004). Previously, we have shown that mice fed a cholesterol-enriched diet exhibited the same effects as 27-OH, up-regulating members of the brain renin-angiotensin system (RAS; Mateos et al., 2009, 2011a,b) and decreasing the levels of activity-regulated cytoskeleton-associated protein (Arc), a key protein in memory consolidation processes (Mateos et al., 2009). Furthermore, decreases in both RAS up-regulation and Arc were also observed in AD brains (Mateos et al., 2009, 2011a).

Cerebral RAS undertakes a role in the regulation of several brain functions such as learning, memory, emotional responses, and processing of sensory information. This role is attributed to the downstream peptide angiotensin IV (AngIV; von Bohlen und Halbach and Albrecht, 2006). AngIV binds with a high affinity to the AngIV receptor identified as the insulin-regulated aminopeptidase (IRAP; Albiston et al., 2001), an enzyme capable of cleaving several bioactive pep-

*M.-A.-M. Ismail and L. Mateos contributed equally to this paper.

Correspondence to Angel Cedazo-Mínguez: Angel.Cedazo-Minguez@ki.se

Abbreviations used: 22(S)-OH, 22S-hydroxycholesterol; 27-OH, 27-hydroxycholesterol; AD, Alzheimer's disease; Arc, activity-regulated cytoskeleton-associated protein; CA, cholic acid; CSF, cerebrospinal fluid; ^{18}F-FDG, ^{18}F-fluorodeoxyglucose; HCD, high-cholesterol diet; ICV, intracerebroventricular; IRAP, insulin-regulated aminopeptidase; LXR, liver X receptor; MWM, Morris water maze; PET, positron emission tomography; RAS, renin-angiotensin system; SUV, standardized uptake value.

The Rockefeller University Press $30.00
J. Exp. Med. 2017 Vol. 214 No. 3 699–717
https://doi.org/10.1084/jem.20160534

tides (Wallis et al., 2007). IRAP is found in specialized vesicles containing the insulin-sensitive glucose transporter (GLUT4) within hippocampal neurons as well as throughout other brain regions, such as the hypothalamus, piriform and entorhinal cortices, pituitary, olfactory bulb, and most neocortical areas, as well as in different nuclei of the limbic and motor systems, including the basal ganglia (Brant et al., 1993; Leloup et al., 1996; El Messari et al., 1998, 2002; Vannucci et al., 1998; Apelt et al., 1999). Both are translocated from these vesicles to the cell surface in response to certain stimuli such as insulin (Fernando et al., 2008), although this translocation does not guarantee GLUT4 activity, as vesicles need also to appropriately fuse to the plasma membrane (Funaki et al., 2004; Leto and Saltiel, 2012). GLUT4 contributes substantially to the uptake of the much-required glucose during memory-related cognitive functions (McNay et al., 2001; McEwen and Reagan, 2004). Likewise, AngIV impacts learning and memory by exhibiting an inhibitory role on IRAP activity (Wright and Harding, 2008).

This evidence prompted us to assess the extent by which 27-OH, a potent regulator of RAS could also modulate glucose uptake in the brain. Our finding sheds light on the mechanism by which high serum cholesterol influences brain glucose metabolism and thereby contributes to cognitive decline in AD and other neurodegenerative disorders. Consequently, we elucidate several key steps suitable for intervention therapeutically.

RESULTS

Cyp27a1 overexpressing mice exhibit decreased glucose metabolism and memory deficits

The enzyme sterol 27-hydroxylase (Cyp27a1) is responsible for converting cholesterol to 27-OH (Båvner et al., 2010). Mice overexpressing the human *Cyp27a1* gene (Cyp27Tg) have five or six times higher levels of 27-OH than control mice (WT) in serum (283 ± 11 vs. 48 ± 2 ng/ml) and in brain (3.5 ± 0.5 vs. 0.3 ± 0.0 ng/mg; $n = 7$; $P = 0.01$). We measured cerebral glucose metabolism in 12-mo-old Cyp27Tg mice by positron emission tomography (PET), using the ^{18}F-fluorodeoxyglucose (^{18}F-FDG) radioligand under isoflurane anesthesia. We have performed all efforts to ensure effective ^{18}F-FDG uptake in the brain. A full description of the used methodology, including its limitations, is included in Materials and methods. The injected dose of ^{18}F-FDG was based on the respective mice weights (Table S1). Cyp27Tg mice showed a lower radioligand uptake compared with their counterpart littermate controls (Fig. 1 A). Further analysis revealed a reduction in ^{18}F-FDG uptake generally across all brain regions of the transgenic mice compared with WT (Fig. 1 B).

Spatial learning and memory retention of 12-mo-old Cyp27Tg mice was assessed using the Morris water maze (MWM) test. No differences in swimming speed or sensory motor functions were found between groups (Fig. 1 C). Spatial learning performance in the MWM test was evaluated by escape latency to the platform. Repeated measures ANOVA did not show significant group effects during the acquisition phase (Fig. 1 D). On day 8, memory was assessed using a probe test. Longer escape latencies suggested a negative effect of *Cyp27a1* gene overexpression on spatial learning performance ($n = 7$–8; $P = 0.02$; Fig. 1 E). Moreover, Cyp27Tg mice performed fewer crossovers on the platform than WT mice ($P = 0.004$) and spent significantly less time in the southeastern quadrant ($n = 7$–8; $P = 0.0008$; Fig. 1, E and F).

Cyp27Tg mice showed decreased expression levels of Arc, a marker of long-term memory consolidation, in both cortex and hippocampus ($P = 0.03$ and $P = 0.02$, respectively; Fig. 1 G), and of GLUT4, a glucose transporter implicated in learning and memory (McEwen and Reagan, 2004; cortex $P = 0.04$ and hippocampus $P = 0.04$; Fig. 1 H). Decreased protein levels of GLUT4 were found in the hippocampus of Cyp27Tg mice (Fig. 1 I). To elucidate whether this effect is dependent on age, samples from 7–8-wk-old Cyp27Tg mice were also analyzed. As seen for 12-mo-old animals, young Cyp27Tg mice exhibited reduced GLUT4 hippocampal levels compared with age-matched WT littermates ($n = 3$–4; 100.0 ± 3.974 vs. 84.93 ± 1.770; $P = 0.0282$).

However, the protein levels of the predominant glucose transporter in neurons, GLUT3 (Vannucci et al., 1997), exhibited no change (Fig. 1 J). Furthermore, the mRNA expression of GLUT1, another glucose transporter abundantly expressed in astrocytes and endothelial cells lining the blood–brain barrier, also revealed no changes in cortical samples from controls (1.000 ± 0.1798) versus Cyp27Tg mice (1.164 ± 0.08593; $P = 0.476$; $n = 3$). All these data suggest that excess 27-OH reduces brain glucose metabolism and disrupts spatial memory retention by a mechanism that could involve the reduction of GLUT4 receptors.

Intracerebroventricular (ICV) injection of 27-OH decreases GLUT4 and Arc in vivo

To investigate if the effects seen in Cyp27Tg animals were caused by the direct influence of 27-OH in the brain, we performed ICV injections of 27-OH (ICV27-OH) in WT animals and measured hippocampal GLUT4 and Arc levels 24 h later. Bilateral ICV injections of 1 µl of a solution containing 10 µM 27-OH resulted in a significant decrease of GLUT4 protein levels ($n = 4$; $P = 0.02$; Fig. 2 A) and Arc expression ($n = 4$; $P = 0.0004$; Fig. 2 B). Notwithstanding a concentration of 5 µM of 27-OH did not induce such changes (Fig. 2, C and D). No significant changes were found in GLUT3 protein levels (Fig. 2 E) between groups. Additionally, ICV injections of 27-OH did not modify the levels of GLUT1mRNA in either cortex (controls 1 ± 0.2625 vs. ICV27-OH 0.8808 ± 0.06755; $P = 0.675$; $n = 3$) or hippocampus (controls 1 ± 0.09894 vs. ICV27-OH 0.7254 ± 0.1104; $P = 0.1004$; $n = 3$).

27-OH reduces glucose uptake and elevates IRAP levels and catalytic activity in vitro

To consolidate the notion that 27-OH plays a direct role in damping neuronal glucose metabolism, we next analyzed the

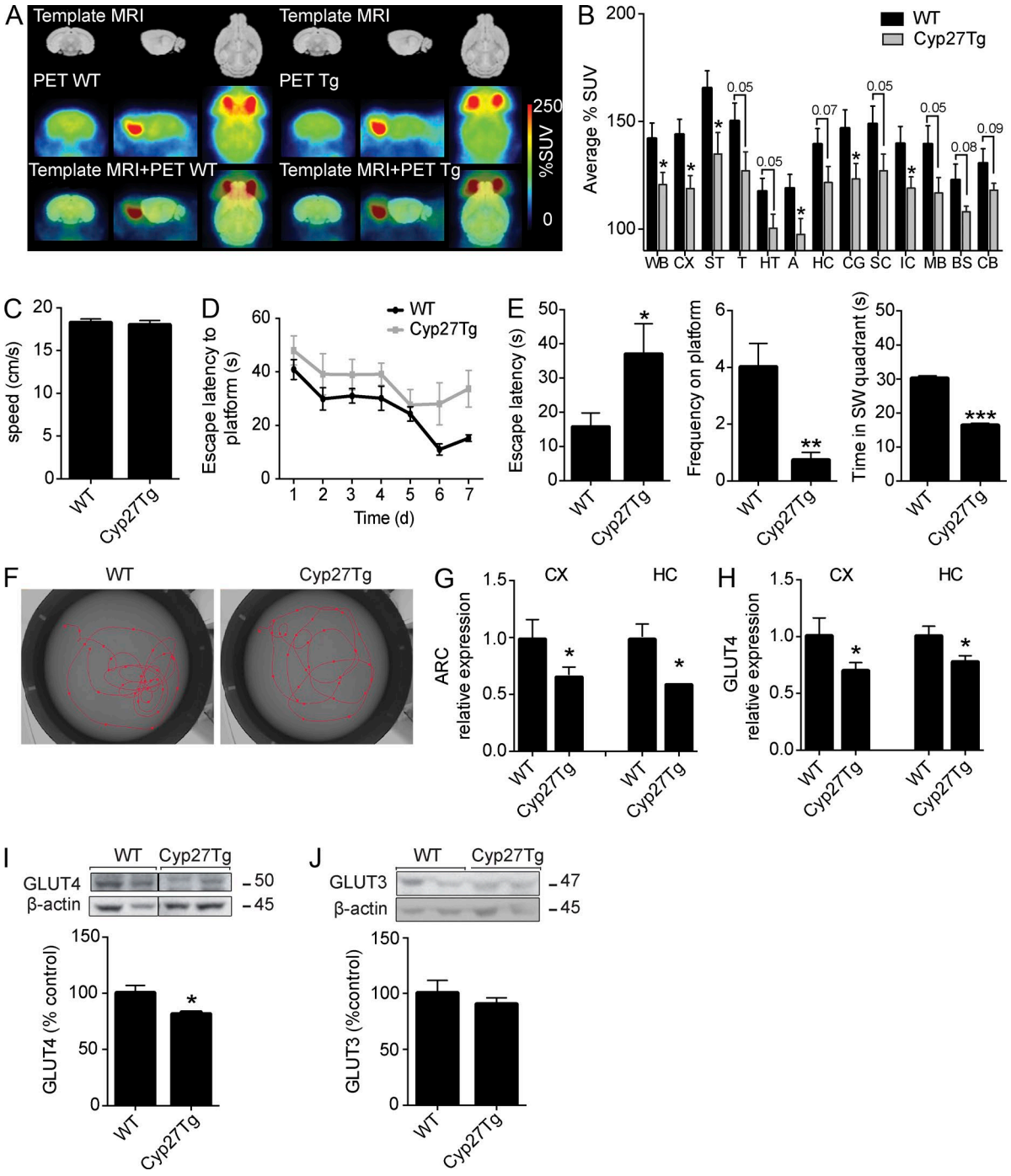

Figure 1. **Cyp27a1-overexpressing mice exhibit decreased glucose uptake and memory deficits.** (A) Representative ^{18}F-FDG PET/MRI images of 12-mo-old *Cyp27a1* mice (Cyp27Tg; C57BL/6 mouse strain) and WT littermate control (n = 4–6) mice. (B) Regional quantification of ^{18}F-FDG uptake in these mice. Testing spatial memory using the MWM task (n = 7–8). (C) Swim speed in the MWM test during two habituation swim trials. (D) Escape latency (i.e., time required to reach hidden platform) over 7-d acquisition phase (repeated-measures ANOVA). (E) Escape latency, frequency to crossover platform, and time spent in the correct quadrant between both groups during probe testing (*, $P < 0.05$; **, $P < 0.005$; ***, $P < 0.0005$; Mann–Whitney U test). (F) Representative panels tracking pathway during probe testing. (G and H) mRNA of Cyp27Tg mice and littermate controls from two brain areas, cortex and hippocampus, analyzed by real-time RT-PCR and normalized to GAPDH as an internal control. Arc (G) and GLUT4(H) mRNA levels from Cyp27Tg mice were lower than in WT mice (n = 3–4). (I and J) Representing immunoblots and quantifications of hippocampal GLUT4 protein levels (I) and GLUT3 protein levels (J) in WT and Cyp27Tg mice (n = 4). Molecular mass is indicated in kilodaltons. All numerical data are presented as mean ± SEM. *, $P < 0.05$; **, $P < 0.01$;

uptake of a fluorescent derivative of glucose, 2-[*N*- (7-nitrobenz-2-oxa-1, 3-diazol-4-yl) amino]-2-deoxy-D-glucose (2-NBDG), in vitro using both rat primary neurons and human neuroblastoma cells (SH-SY5Y). Glucose uptake was reduced in rat primary neurons in presence of 1 μM 27-OH (24 h) to ∼70% in relation to controls ($n = 21$; $P < 0.0001$; Fig. 3 A). Insulin, a positive control, increased 2-NBDG uptake. Furthermore, 27-OH managed to reduce the insulin-mediated glucose uptake ($n = 12$; $P < 0.0001$). Similar results were found in SH-SY5Y cells where 27-OH reduced glucose uptake by 76% of control ($n = 12$; $P < 0.0001$). Because GLUT4 and IRAP are functionally intimately related (Fernando et al., 2008), we also analyzed the effects of 27-OH on GLUT4 and IRAP expressions in cortical and hippocampal primary neurons. A reduction in GLUT4 and an enhancement in IRAP mRNA and protein levels were found after 27-OH treatments (Fig. 3, B–E). Furthermore, no difference was found in neuronal GLUT3 levels (Fig. 3 F).

As we have previously reported (Mateos et al., 2011b), 27-OH is a well-known endogenous ligand of liver X receptors (LXRs). To explore whether the effects of 27-OH on IRAP is LXR dependent, pretreatment with an LXR antagonist, 22S-hydroxycholesterol (22(S)-OH; 10 μM), blocked 27-OH–induced IRAP up-regulation (Fig. 3 G; $n = 4$; $P = 0.019$). Suppression of LXRβ by siRNA (Fig. 3 H, left) ameliorated the effects of 27-OH on IRAP expression ($P = 0.0159$; Fig. 3 H, right), further confirming that 27-OH regulates the expression of IRAP by an LXR-dependent mechanism. 27-OH treatment also significantly increased IRAP catalytic activity in extracts of membrane proteins from cortical (Fig. 3 I; $n = 19$; $P < 0.0001$) and hippocampal primary neurons (Fig. 3 J; $n = 20$; $P < 0.0001$).

GLUT4 is an insulin-mediated glucose uptake receptor. Thus, it is imperative to scrutinize the effect 27-OH has on insulin signaling. To this end, we investigated the phosphorylation of both insulin receptor and AKT. In our in vivo paradigms, Cyp27Tg and ICV27-OH, no differences were seen compared with their respective controls (Fig. 4, A and B). Furthermore, in vitro, together with insulin, 27-OH seemed to have no effect on hindering insulin receptor phosphorylation, although it did accentuate AKT phosphorylation (Fig. 4 C).

Effects of AngIV on glucose uptake and IRAP catalytic activity are countered by 27-OH

Considering that 27-OH influences the upstream RAS pathway and the receptor of AngIV, IRAP, we hypothesized that precursor enzymes of AngIV maybe be implicated as well. 27-OH treatment more than doubled the expression of AP-A and AP-N in rat primary neurons ($n = 9$; $P < 0.05$ and $P < 0.01$, respectively; Fig. 5 A). This effect was mediated by an LXR-dependent mechanism because pretreatment with 22(S)-OH abolished AP-A and AP-N up-regulation in the presence of 27-OH (Fig. 5 B).

AngIV stimulates glucose uptake by increasing the exposure of IRAP and GLUT4 at the cell surface (Vanderheyden, 2009). As expected (Fernando et al., 2008), 1 μM AngIV enhanced glucose uptake in SH-SY5Y cells, although this effect was abolished when cells were co-treated with 27-OH ($n = 9$; $P < 0.001$; Fig. 5 C). This increase with AngIV was also observed in rat primary culture (141% compared with control; $n = 26$; $P < 0.001$). In contrast to the findings of a previous study (Lew et al., 2003), we could not see that AngIV inhibits IRAP catalytic activity (Fig. 5 D). However, we observed that treatment with AngIV damped the effect exerted by 27-OH on IRAP catalytic activity ($n = 15$; $P < 0.001$; Fig. 5 D). Furthermore, AngIV did not change the expression of GLUT4 but did enhance IRAP mRNA levels ($n = 6$; $P < 0.001$; Fig. 5 E).

27-OH effects on glucose uptake and IRAP catalytic activity are mediated by AP-A and AP-N

One mechanism by which 27-OH impairs glucose uptake and IRAP activity is by maybe altering the balance between AngIII and AngIV. Thus, we used bestatin, an inhibitor of a range of metallo-aminopeptidases shown to hinder AngIV production and induce AngIII accumulation (Abhold et al., 1987). Bestatin treatment resulted in changes similar to 27-OH on glucose uptake ($n = 6$; $P < 0.001$), IRAP activity ($n = 19$; $P < 0.0001$), and GLUT4 and IRAP mRNA levels ($n = 4$; $P < 0.05$ and $P < 0.001$, respectively; Fig. 6, A–C). To test whether AngIII specifically exerts such a function, cementing its active role rather than a mere intermediary role, as previously thought (Yugandhar and Clark, 2013), we used two strategies. First, treatment with AngIII induced similar effects as 27-OH, displaying reduced glucose uptake ($n = 12$; $P = 0.03$) and increased IRAP activity ($n = 3$–6; $P < 0.0001$; Fig. 6, D and E). Moreover, in neurons with depressed generation of AngIII (by silencing AP-A mRNA expression; Fig. 6 F), the 27-OH effects on glucose uptake (Fig. 6 D), IRAP catalytic activity (Fig. 6 E), and GLUT4 and IRAP expression (Fig. 6 G) were eliminated. Additionally, knocking down AP-A also abolished the bestatin-mediated increase in IRAP catalytic activity (Fig. 6 H). Furthermore, reducing AngIV degradation by siRNA reduction of AP-N expression also abolished the effects of 27-OH on both IRAP and GLUT4 expression (Fig. 6, I and J).

AP-N and IRAP in *Cyp27a1* overexpression, ICV27-OH, and sterol 27-hydroxylase–deficient mice

Here, we aimed to check whether the high levels of 27-OH in vivo mirrored the same findings as the in vitro results.

***, $P < 0.001$ (unless otherwise noted, an unpaired Student's two-tailed *t* test was used to compare the two conditions). The indicated sample size resulted from one (A–F) or three (G–J) independent experiments. A, amygdala; BS, brainstem; CB, cerebellum; CG, central gray; CX, cortex; HC, hippocampus; HT, hypothalamus; IC, inferior colliculi; MB, midbrain; SC, superior colliculi; ST, striatum; T, thalamus; WB, whole brain.

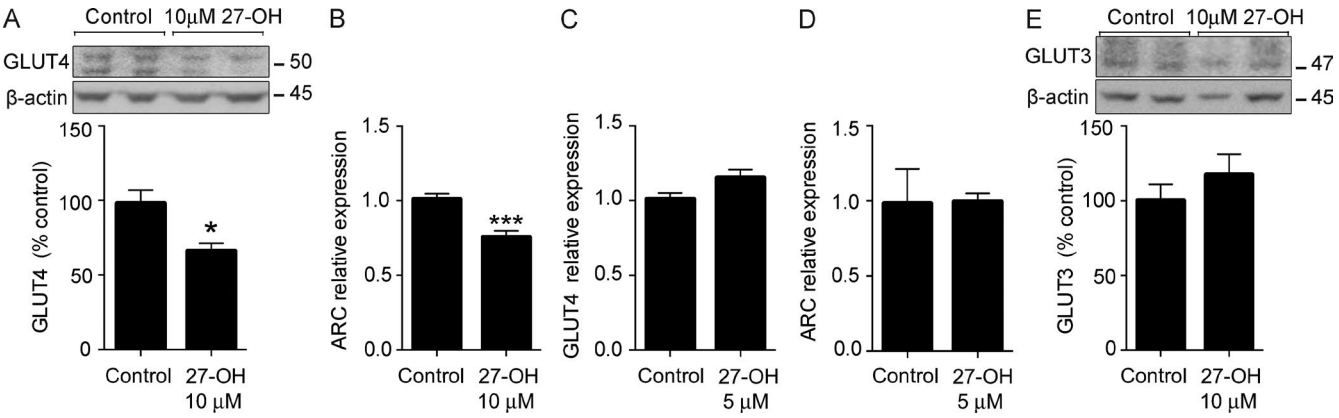

Figure 2. **Further characterization of the 27-OH ICV injected mice.** (A and B) ICV injections of 10 μM 27-OH (ICV27-OH) were made into the lateral ventricle of 7–8-wk-old C57BL/6 WT mice. The hippocampi of the mice were then analyzed by Western blot for GLUT4 protein (A) and RT-PCR for Arc mRNA levels (B; $n = 4$). (C and D) The ICV injections of 5 μM 27-OH in WT mice were similarly analyzed by RT-PCR for RNA expression levels of both GLUT4 (C) and Arc (D) in the hippocampus. (E) Western blot showing GLUT3 levels in 10 μM 27-OH–injected WT mice. (A and E) Molecular mass is indicated in kilodaltons. All numerical data are presented as mean ± SEM. *, $P < 0.05$; ***, $P < 0.001$ (unpaired Student's two-tailed *t* test). The indicated sample size ($n = 4$) resulted from two independent experiments.

Cyp27Tg mice exhibited increased IRAP ($P = 0.024$), AP-A ($P = 0.05$), and AP-N ($P = 0.005$) mRNA levels ($n = 4$; Fig. 7 A). Immunoblotting analysis confirmed an increase in IRAP protein levels in Cyp27Tg mice compared with WT mice ($n = 3$–4, $P = 0.0121$; Fig. 7 B). Membrane protein preparations from Cyp27Tg showed higher IRAP catalytic activity compared with WT mice ($n = 19$; $P < 0.0001$; Fig. 7 C). Similar results were found in the hippocampus of 10 μM ICV27-OH–injected WT mice (Fig. 7, D–F). On the contrary, as seen in Fig. 7 (G–I), sterol 27-hydroxylase–deficient mice ($Cyp27^{-/-}$) expressed lower levels of 27-OH, and brain samples showed a significant reduction in AP-N expression ($n = 4$; $P = 0.05$) and IRAP activity ($n = 19$; $P < 0.0001$); however, IRAP levels were comparable to WT animals.

Similarly to the ICV27-OH mice injected with 10 μM, mice injected with 5 μM also revealed higher levels of IRAP and AP-N mRNA levels though AP-A was decreased and no change in IRAP protein levels was observed (Fig. 8, A and B).

Consequently, HCD-fed mice showed a significant increase in IRAP catalytic activity compared with animals on normal diet ($n = 19$; $P < 0.0001$; Fig. 8 C). The cholesterol plasma levels were doubled in HCD-fed animals compared with controls (2.78 ± 0.55 vs. 1.51 ± 0.56 mmol/liter; $P = 0.0011$). In an attempt to modify the pattern seen in the $Cyp27^{-/-}$ mice and prove the involvement of LXR, we fed $Cyp27^{-/-}$ mice a diet supplemented with a known LXR agonist, cholic acid (CA; Theofilopoulos et al., 2013). The level of CA was found to be 14 ± 7 ng/g (mean ± SEM; $n = 3$) in the brains of $Cyp27^{-/-}$ mice on the control diet and 42 ± 4 ng/g in the brains of $Cyp27^{-/-}$ mice treated with the diet enriched with CA, indicating that dietary CA can effectively enter the brain. LXR activation in $Cyp27^{-/-}$ mice recovered IRAP catalytic activity levels to control (WT) levels (Fig. 8 D). Moreover, treatment with CA significantly increased the expression of IRAP, AP-A, and AP-N in the brains of $Cyp27^{-/-}$ mice ($n = 4$; $P < 0.01$; Fig. 8 E).

Glucose uptake deficits in patients linked to the levels of 27-OH

To translate in humans whether high 27-OH levels are associated with reduced brain glucose metabolism, we measured 27-OH in CSF and cerebral glucose metabolism in patients with varying degrees of cognitive impairment (Table S2).

Despite the small number of patients in the study ($n = 21$), a significant negative correlation between 27-OH and ^{18}F-FDG uptake was observed in the hippocampus ($P = 0.011$), posterior cingulate ($P = 0.05$), and cerebellum ($P = 0.04$; Fig. 9 A). For additional statistical analysis, we stratified the cohort into two groups according to the concentration of 27-OH in CSF. A global decrease in brain ^{18}F-FDG uptake was observed in patients possessing >1 ng/ml 27-OH as compared with patients with lower levels (Fig. 9 B). Decreased ^{18}F-FDG uptake in patients with ≥1 ng/ml 27-OH in CSF was found in the hippocampus and posterior cingulate, but not in the cerebellum (Fig. 9 C), compared with those with lower CSF 27-OH levels.

DISCUSSION

Dysregulated metabolism of brain cholesterol is associated with progressive neurodegenerative disorders, including AD and other dementia-causing diseases (Björkhem et al., 2009). However, no causal link between altered cholesterol metabolism and decreased cognition has yet been identified. Our findings implicate 27-OH, a peripherally produced cholesterol metabolite, in the reduction of brain glucose uptake by modifying the activity of the IRAP–GLUT4 complex, exposing a previously unknown cross-talk between blood cholesterol and memory-related brain processes. Substantial

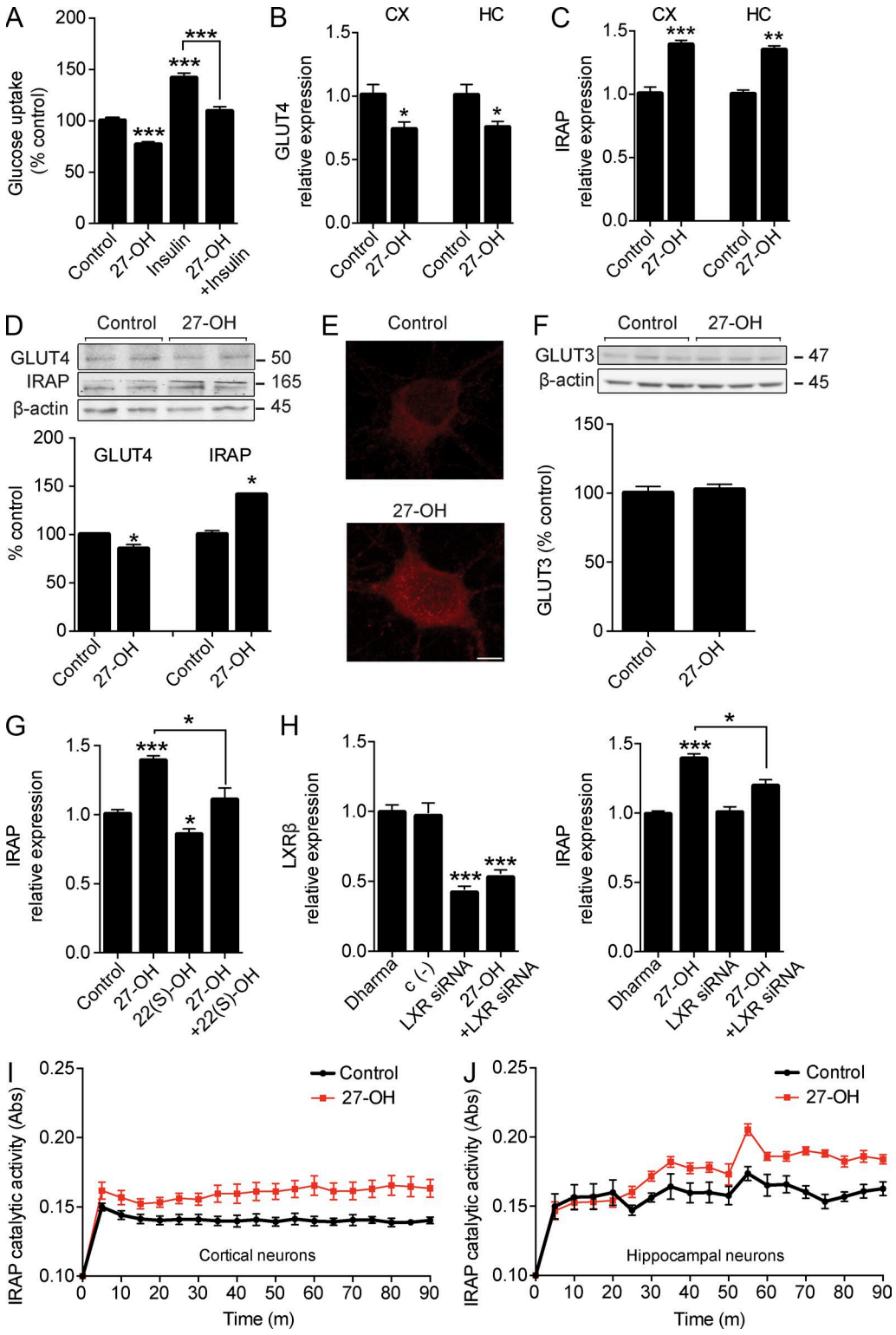

Figure 3. **27-OH reduces glucose uptake and elevates IRAP levels and catalytic activity in vitro.** (A) Rat primary cortical cultures were treated with 1 µM 27-OH (24 h), 100 nM insulin (3 h), or both (insulin was used as a positive control). The fluorescent glucose analogue 2-NBDG (2-[N- (7-nitrobenz-2-oxa-1, 3-diazol-4-yl) amino]-2-deoxy-D-glucose) was used at 100 µM diluted in HBSS. After incubation at 37°C for 1 h with the analogue in addition to the treatments, culture medium was removed and fluorescence was measured (n = 21). (B and C) GLUT4 and IRAP mRNA levels in cortical (CX) and hippocampal (HC) rat primary neurons treated with 27-OH (n = 6). (D) Rat primary cortical neuron lysates treated with 27-OH immunoblotted

glucose requirements were observed during memory processing, especially in the hippocampal region (McNay et al., 2001), and glucose hypometabolism is a feature of several cognition-affecting neurodegenerative disorders (Teune et al., 2010). The behavior of Cyp27Tg mice revealed a deficit in memory-related tests in addition to reduced uptake of glucose disclosed by ^{18}F-FDG PET and levels of GLUT4. Decreased GLUT4 levels were also found in ICV injected 27-OH animals. However, the expression of the more abundant glucose transporters, neuronal GLUT3 and astrocytic/endothelial GLUT1, was not changed in both in vivo models (i.e., Cyp27Tg and ICV27-OH). Consistent with the notion that synaptic connectivity bears the largest demand for energy in the brain (Attwell and Laughlin, 2001) and based on the kinetic characteristics and the cellular concentration of glucose in both neurons and glia, the capability of glucose transport in neurons (via GLUT3 and GLUT4) surpasses that of astrocytic GLUT1 (Simpson et al., 2007). To date, or unbeknown to us, the GLUT4-mediated glucose uptake in the brain has not been quantified, nor has the extent of its contribution to glucose metabolism been established. Our results are in agreement with the notion that 27-OH affects insulin-mediated glucose uptake (mainly dependent on GLUT4), which has a major impact on brain functioning.

We have previously reported that higher 27-OH levels result in over-activation of brain RAS (Mateos et al., 2011b). A recognized function of AngIV, one of the RAS metabolites, is to facilitate learning and memory (De Bundel et al., 2010). This enhanced cognitive processing is speculated to result from the promotion of glucose uptake by neurons (De Bundel et al., 2009; Vanderheyden, 2009) or the binding of AngIV to IRAP reducing its cleavage of memory-enhancing neuropeptides (Wright and Harding, 2008). On the contrary, the precursor peptide of AngIV, AngIII, is proposed to play a predominant role in regulation of blood pressure, exerting a central tonic stimulatory control in hypertensive animals (Gao et al., 2014). Our results, summarized in Fig. 10, demonstrate that excessive 27-OH brain levels enhance IRAP and reduce GLUT4 activities. It seems likely that a correct balance between the IRAP activator/GLUT4 inhibitor AngIII and the IRAP inhibitor/GLUT4 activator AngIV is key for the modulation of IRAP and GLUT4 functions. We demonstrate that AngIII and AngIV exert opposing functions on regulating IRAP catalytic activity and GLUT4-dependent glucose uptake. Such a balance would depend on the activity of not only aminopeptidases converting AngIII to AngIV but also of those degrading AngIV. In this complex process, AP-N seems to have a key role. As reviewed by Stragier et al. (2008), processing of AngIV into smaller peptide fragments is predominantly achieved by AP-N, a membrane-bound Zn^{2+} aminopeptidase involved in angiogenesis, tumorigenesis, and immune system response (Luan and Xu, 2007) but, so far, not in neurodegenerative disorders.

We demonstrate that 27-OH is able to restrain the ability of AngIV to stimulate glucose uptake and inhibit IRAP catalytic activity. This novel function of 27-OH is mediated by LXRβ up-regulation of AP-N, as using the LXR inhibitor 22(S)-OH or reducing LXRβ or AP-N expression counters the effects of 27-OH. Furthermore, the LXR-agonist CA reverted the effects of down-regulating the production of 27-OH in mice. In agreement with our findings, an LXR agonist, GW3965, down-regulates insulin-stimulated glucose uptake in adipocytes through a GLUT4-dependent mechanism (Pettersson et al., 2013). Up-regulation of AP-N can be expected to result in increased cleavage of AngIV into other peptides and accordingly, a reduction of the IRAP inhibitory/GLUT4 stimulatory functions of AngIV. Consistent with the effects seen in vitro, Cyp27Tg mice displayed higher and Cyp27$^{-/-}$ mice lower levels of AP-N. The catalytic activity of IRAP reflected those alterations, respectively. Conversely, bestatin, reported to reduce metabolism and prolong the effects of AngIII in vivo (Abhold et al., 1987) and hence lower AngIV levels, also mimicked 27-OH, increasing IRAP expression and catalytic activity while decreasing GLUT4 expression and glucose uptake. In support of this notion, AngIII produced similar results to bestatin. Moreover, loss of function of AngIII by knocking down AP-A resulted in the return to control levels. This identifies 27-OH as an important modulator of AP-A and AP-N and hence of the balance between beneficial AngIV and the seemingly negative AngIII effects on glucose metabolism and IRAP activity.

Because IRAP potentially cleaves a large number of substrates (Saveanu and van Endert, 2012), pathologically enhanced activity of this enzyme would exert a wide range of central and peripheral effects, such as hypertension (Goldstein et al., 2008) and decreased levels of somatostatin (Burgos-Ramos et al., 2008) or arginine vasopressin (Rossor et al., 1980; Mazurek et al., 1986). Notably, an enhanced cleavage of

against IRAP and GLUT4 on separate representative membranes. Histogram shows data normalized as ratio to actin levels and expressed as percentage of control (n = 6). (E) Confocal microscopy of primary cortical neurons (control and 1 µM 27-OH treated [24 h]) stained against IRAP (red). Bar, 5 µm. (F) GLUT3 protein levels in 27-OH–treated primary neurons compared with controls (n = 3). (D and F) Molecular mass is indicated in kilodaltons. (G) IRAP mRNA levels in rat primary cortical neurons pretreated with an LXR blocker, 10 µM 22(S)-OH (3 h), and 1 µM 27-OH (24 h; n = 4). (H) LXRβ was knocked down in primary cortical cultures using siRNA. LXRβ mRNA levels confirm knockdown efficiency (left). IRAP mRNA expression levels in LXRβ–knocked down neurons treated with 27-OH (right; n = 4). (I and J) Membrane extracts from rat cortical (n = 19; P < 0.0001; I) and hippocampal (n = 20; P < 0.0001; J) primary neurons were used to analyze the enzymatic cleavage of L-Leu-pNA in the presence of 27-OH, mirroring IRAP catalytic activity (paired two-tailed Student's t test). All data are presented as mean ± SEM; *, P < 0.05; **, P < 0.01; and ***, P < 0.001. Unless otherwise stated, an unpaired Student's two-tailed t test was used to compare control and treatment conditions. The indicated sample size was obtained from six (I and J), four (A), three (B–F), and two (G and H) independent experiments.

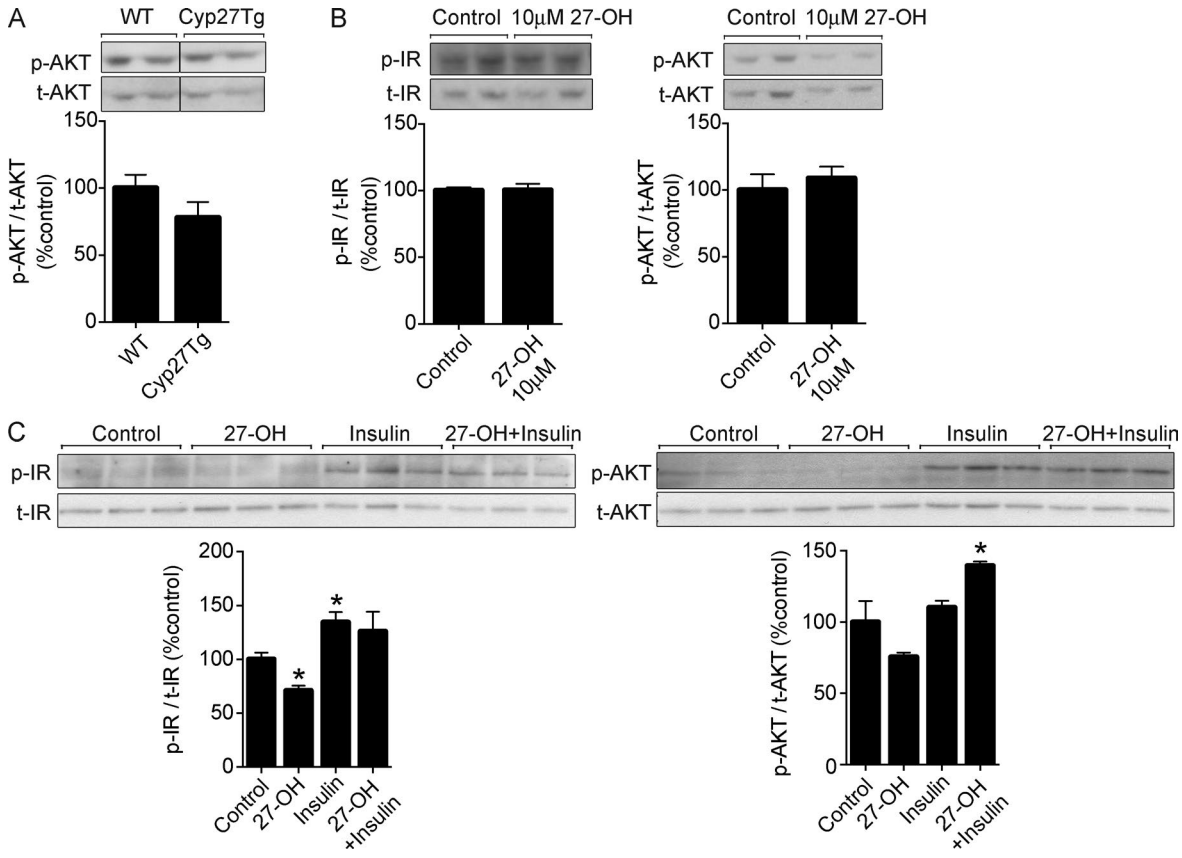

Figure 4. **Insulin signaling in the presence of 27-OH.** (A) Representative immunoblot of Cyp27Tg and WT mice (n = 4–5) showing phosphorylated AKT (p-AKT) and total AKT (t-AKT). Histogram indicates the ratio between phosphorylated and t-AKT. (B) Western blot of mice injected with 10 µM 27-OH or artificial CSF (control) in the lateral ventricle (n = 4). Representative blots show phosphorylated insulin receptor (p-IR) and p-AKT along with their total forms (t-IR and t-AKT), whereas histograms indicate the ratio between the phosphorylated and total protein. (C) Rat primary neurons treated with 1 µM 27-OH (24 h) and/or 100 nM insulin (for the last 3 h) were blotted with p-IR and p-AKT (n = 3). Histograms indicate the ratio between phosphorylated and their counterpart total protein. p-AKT and t-AKT were detected at ∼60 kD, whereas p-IR and t-IR were detected at ∼95 kD. Data are presented as mean ± SEM; *, $P < 0.05$ (unpaired Student's two-tailed t test as compared with control). The indicated sample size was obtained from two (A and B) or three (C) independent experiments.

neuropeptides by IRAP is proposed to contribute to deteriorating memory processing (Lew et al., 2003).

In principle, the effects seen in the brain caused by high plasma cholesterol or its metabolites may be caused by peripheral mechanisms rather than by direct effects on the brain. To exclude that peripheral effects are of major importance, we injected 27-OH directly into the lateral ventricle of WT mice. This led to similar alterations as seen in the Cyp27Tg mice, i.e., a decrease in GLUT4 and Arc expression while increasing AP-A, AP-N, and IRAP levels. 27-OH levels are closely correlated to cholesterol in the circulation (Björkhem et al., 2006), and most likely hypercholesterolemia is accompanied by an increased influx of 27-OH into the brain. In accordance with this notion, HCD-fed mice exhibit increased IRAP catalytic activity in the brain (Fig. 8 C). We report a negative correlation between 27-OH levels and brain glucose uptake in patients suffering variant cognitive impairments. Of note, patients had normal cholesterol levels and were not taking cholesterol-lowering drugs. However, a high proportion of these patients had relatively high CSF levels of 27-OH, indicating a high cholesterol metabolic rate. Although these results do not reveal any causality, they do indicate a tendency, and more comprehensive studies are needed to assess whether high cholesterol metabolizers have an increased risk of glucose hypometabolism. In support of this notion, it is well documented that aberrant CSF levels of 27-OH are found in patients with mild cognitive impairment (Leoni and Caccia, 2011; Mateos et al., 2011a) and that 27-OH accumulates in the brain of AD patients (Heverin et al., 2004).

Cyp27a1 inhibitors may therefore be of greater benefit than statins in reducing the risk of dementia. This study validates mechanistically the use of IRAP inhibitors that were shown to improve memory (Albiston et al., 2008) and also supports the use of AP-N inhibitors while challenging the benefits of LXR agonists for dementia patients. These new

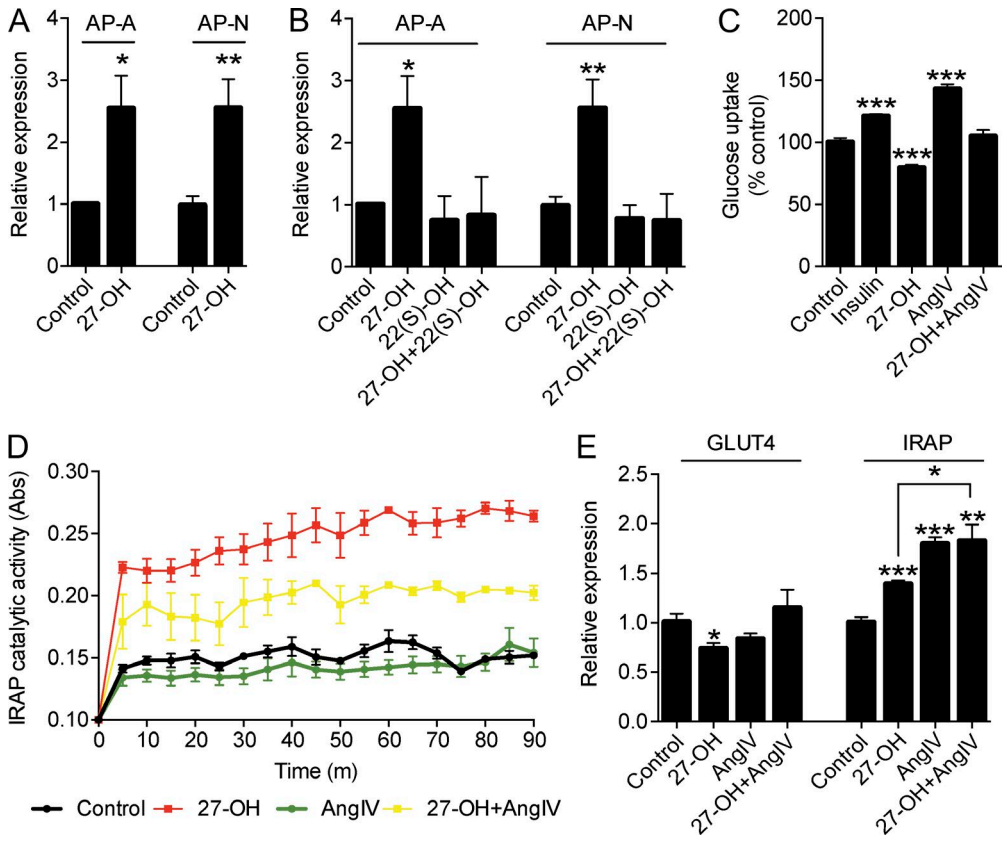

Figure 5. **Effects of AngIV on glucose uptake and IRAP catalytic activity are countered by 27-OH.** (A) mRNA levels of AP-A and AP-N, respectively, in rat primary cortical neurons treated with 1 µM 27-OH (24 h) compared with nontreated cells (n = 9). (B) AP-A and AP-N mRNA levels in rat primary cortical neurons pretreated with an LXR blocker, 10 µM 22(S)-OH (3 h; n = 3–6). (C) Glucose uptake measured by 2-NBDG in human neuroblastoma cells (SH-SY5Y). The treatments include 1 µM AngIV (3 h) in addition to 1 µM 27-OH (24 h) and 100 nM insulin (3 h; n = 9–12). (D) IRAP catalytic activity was measured by the enzymatic cleavage of L-Leu-pNA in the presence of 1 µM AngIV (3 h), 1 µM 27-OH (24 h), or both in rat primary neurons (n = 15; $P < 0.001$, paired two-tailed Student's t test). (E) GLUT4 and IRAP mRNA levels evaluated after treatments with AngIV and AngIV + 27-OH (n = 6). Data are shown as mean ± SEM; *, $P < 0.05$; **, $P < 0.01$; ***, $P < 0.001$. Unless otherwise noted, an unpaired Student's two-tailed t test was used to compare control and treatment conditions. The indicated sample size was obtained from at least three independent experiments.

targets may lead the way to alternative therapeutic strategies hindering the advancement of AD.

Although shedding light on the interplay of risk factors (hypercholesterolemia, hypertension, and glucose dysmetabolism) in the pathogenesis of dementia, our study has some limitations, as it does not address the reversibility of these effects and does not include interventions against the therapeutic targets identified such as Cyp27a1, IRAP, or AP-N. Furthermore, the patient sample size is considerably small, although it provided us a proof of concept; a more comprehensive cohort would be required to consolidate this notion of 27-OH being a biomarker for reduced glucose metabolism.

MATERIALS AND METHODS

Study design

The objective of the study was to determine whether 27-OH, a peripheral cholesterol metabolite, could influence brain glucose metabolism and to elucidate its mechanism. The stated hypothesis was investigated by incorporating mice models, cell cultures, and a patient cohort. Mice models consisted of Cyp27a1 overexpression (Cyp27Tg) and knockout mice ($Cyp27^{-/-}$), HCD-fed mice, $Cyp27^{-/-}$ mice treated with an LXR-agonist and mice intracerebroventricularly injected with 27-OH. PET-scanned patients were randomly selected and are described in detail below (see Human patient data and Human ^{18}F-FDG PET imaging sections). ^{18}F-FDG PET scanning of both Cyp27Tg and patients assessed glucose metabolism in addition to measurements made in vitro with various treatments using a fluorescent glucose analogue. Several biological techniques were used to explore the mechanistic aspect of the study.

Animals

Generation and breeding of both the Cyp27Tg and $Cyp27^{-/-}$ mice has been described previously (Meir et al., 2002; Båvner et al., 2010). WT mice were fed an HCD containing 21% fat

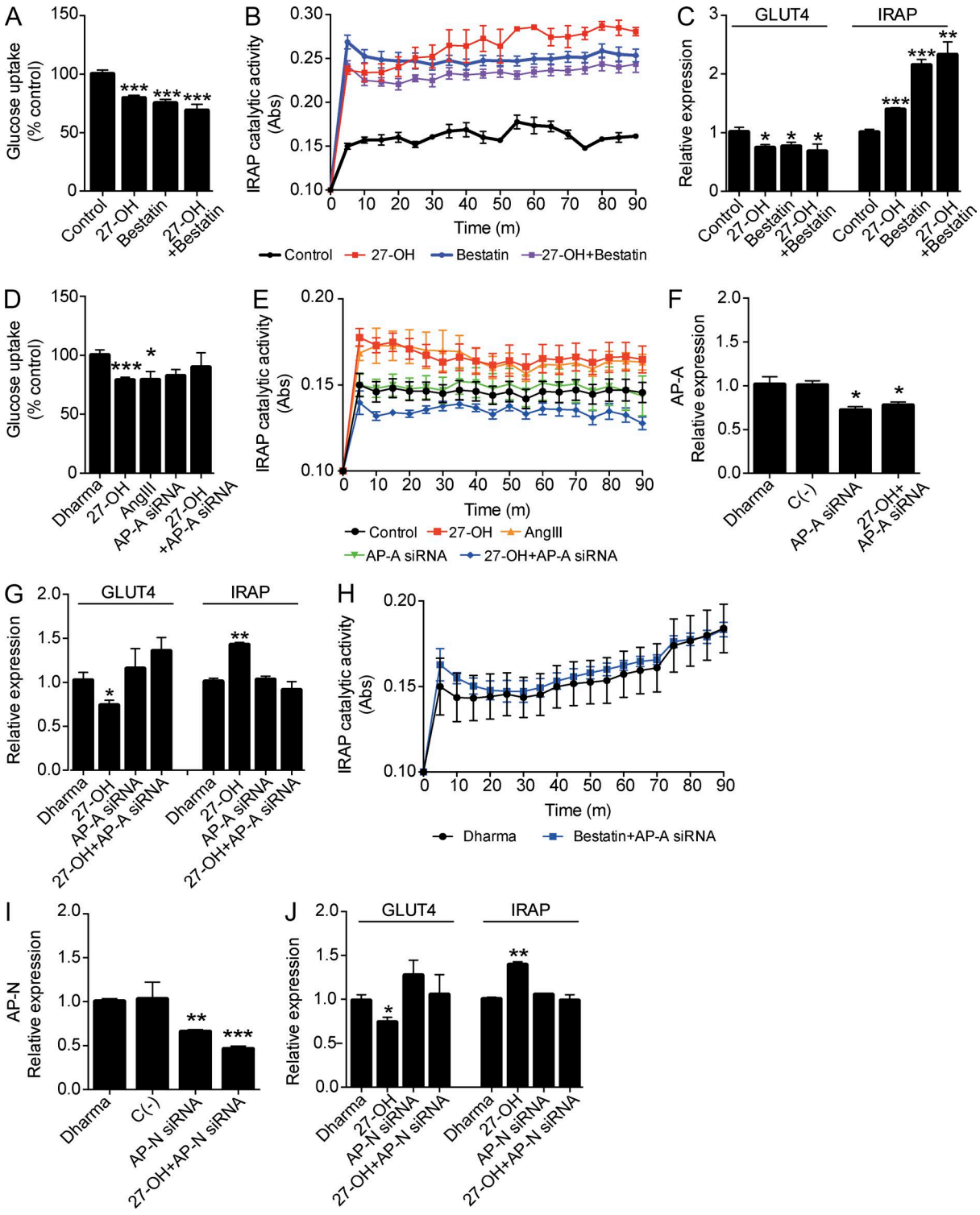

Figure 6. **27-OH effects on glucose uptake and IRAP catalytic activity are mediated by AP-A and AP-N.** (A and B) Bestatin, a metallo-aminopeptidase inhibitor, hinders AngIV production and induces AngIII accumulation. Treatment with 10 µM bestatin (24 h) was analyzed by measuring glucose uptake ($n = 6$; A) and IRAP catalytic activity ($n = 19$; $P < 0.0001$; B). (C) Quantification of GLUT4 and IRAP mRNA levels by real-time RT-PCR after bestatin treatment ($n = 4$). (D) Glucose uptake was measured with treatments of 1 µM AngIII (3 h) in addition to the loss of function of AngIII achieved by siRNA knockdown of AP-A ($n = 12$). (E) IRAP catalytic activity observed with AngIII treatments and in knocked down AP-A neurons ($n = 3–6$; $P < 0.0001$). (F) AP-A mRNA levels showing knockdown efficiency using AP-A siRNA ($n = 3$). (G) RT-PCR showing the mRNA expression of both GLUT4 and IRAP in AP-A–knocked

and 0.15% cholesterol (R638, lactamine) for 9 mo. A subset of Cyp27$^{-/-}$ mice were treated with 0.05% CA for 16 wk. ICV27-OH mice are described in more detail below (see Stereotaxic injections section). C57BL/6 is the background mouse strain of all the mice used in the study. Ethical consent was received from the Southern Stockholm Research Animal Ethics Committee. Animals were sacrificed by decapitation and the brains immediately frozen on dry ice and stored at −80°C until further analysis. WT littermate controls were used in all experiments using genetically modified mice.

Human patient data

75 patients, who underwent brain ^{18}F-FDG PET imaging at the Department of Radiology, Karolinska University Hospital, were selected at random. All patients were investigated according to the procedures at the memory clinic at Karolinska Hospital, Huddinge, Sweden. Neurological and psychiatric evaluation was performed, including a comprehensive cognitive evaluation by a neuropsychologist. Diagnoses were assessed according to International Classification of Diseases, 10th Revision (World Health Organization, 1992). 34 subjects only had CSF available in addition to Aβ-42, t-tau, and p-tau analysis. There was no stratification of the patient sample based on diseases, and hence a heterogeneous group of neurological diseases was present. Because of the clinical setting of the PET scanning, a stricter research criterion was used to ensure accurate observations. Thus, to reduce variations of standardized uptake value (SUV) levels, 11 patients were excluded as the time between injection of the radioligand and scanning exceeded 45 min or was <30 min. Two patients were also excluded as their lipid status and sequential use of cholesterol modifying medication may confound data. The regional human ethics committee of Stockholm approved the study, and all subjects gave their informed consent.

Human ^{18}F-FDG PET imaging

Brain ^{18}F-FDG PET of 21 patients was retrospectively analyzed. PET scans (10 min long) were performed 30–45 min after intravenous injection of 3 MBq/kg weight (198–320 MBq). PET scans were obtained with a Biograph mCT (Siemens) PET/CT having a 21.6-cm field of view (FOV) providing 148 contiguous 1.47-mm slices producing a pixel size of 1.02 mm. A low-dose CT scan was used for attenuation correction of PET data. All appropriate corrections, including time-of-flight (TOF), were applied. Reconstruction was done with ordered subset expectation maximization (OSEM; 5 iterations, 21 subsets, 2.0-mm Gaussian filter). The effective resolution of the images is 3 mm.

A quantitative analysis of PET scans was performed using *syngo*.via program (Siemens). An automated volume-of-interest (VOI)–based analysis of FDG uptake (SUVR) for the hippocampal, parietal, frontal, temporal cortical regions as well as posterior cingulate was applied. A comparison of brain metabolism with healthy age-matched individuals was done with automated Z score method (3D-SSP) using cerebellum as a reference region.

Isolation and culture of rat primary neurons

Primary cortical and hippocampal neuronal cultures from embryonic day (E) 18 Sprague Dawley rat embryos were established as described previously (Mateos et al., 2009). 27-OH was obtained from Steraloids, and treatments were done at 1 μM for 24 h. Blocking LXR was done by preincubating cells for 3 h with 10 μM 22(S)-OH (Sigma-Aldrich). AngIV and AngIII (Bachem) treatments were added at 1 μM in the last 3 h of 27- OH treatment. Furthermore, 10 μM bestatin (Sigma-Aldrich) was added for 24 h or co-incubated with 27-OH. Insulin signaling experiments were done by incubating 1 μM 27-OH for 24 h, and 100 nM insulin was added in the last 3 h. Experiments with primary cultures were conducted following approval from the regional ethical committee of Karolinska Institutet, Stockholm.

Immunoblotting analyses

Quantified, using the BCA protein assay kit (Thermo Fisher Scientific), equal amounts of protein were separated using 10% SDS-PAGE. After transfer to a nitrocellulose membrane (Schleicher & Schuell), milk-blocked blots were incubated with IRAP (#3808S; Cell Signaling Technology), GLUT4 (#2213; Cell Signaling Technology), GLUT3 (ab41525; Abcam), and actin antibody (#A2066; Sigma-Aldrich) overnight at a 1:1,000 dilution. Insulin signaling was investigated using the following primary antibodies: phosphorylated (Ser473)-AKT (#4051; Cell Signaling Technology), phosphorylated insulin receptor (Tyr1150/1150, #3024; Cell Signaling Technology), Pan-AKT (#2920; Cell Signaling Technology), and insulin receptor β (#3020; Cell Signaling Technology). Secondary incubation was done using anti–rabbit or anti–mouse IgG at a 1:2,000 dilution (GE Healthcare). Immunoreactivity was detected by the ECL detection system (GE Healthcare). The densitometric analyses of the immunoreactive bands were performed using ImageJ software (National Institutes of Health).

down neurons. (H) IRAP catalytic activity of AP-A–knocked down rat primary neurons treated with bestatin (n = 3). (I) AP-N was knocked down using siRNA. The efficiency of AP-N knockdown was assessed using RT-PCR. (J) GLUT4 and IRAP mRNA expression levels in AP-N–knocked down neurons (n = 3). Transcription levels were normalized to GAPDH mRNA levels. All experiments were performed in rat primary neurons. Data are mean ± SEM; *, $P < 0.05$; **, $P < 0.01$; ***, $P < 0.001$. Unpaired Student's two-tailed t test was used for all comparisons except IRAP catalytic activity, where a paired Student's t test was used. The indicated sample size was obtained from at least three independent experiments.

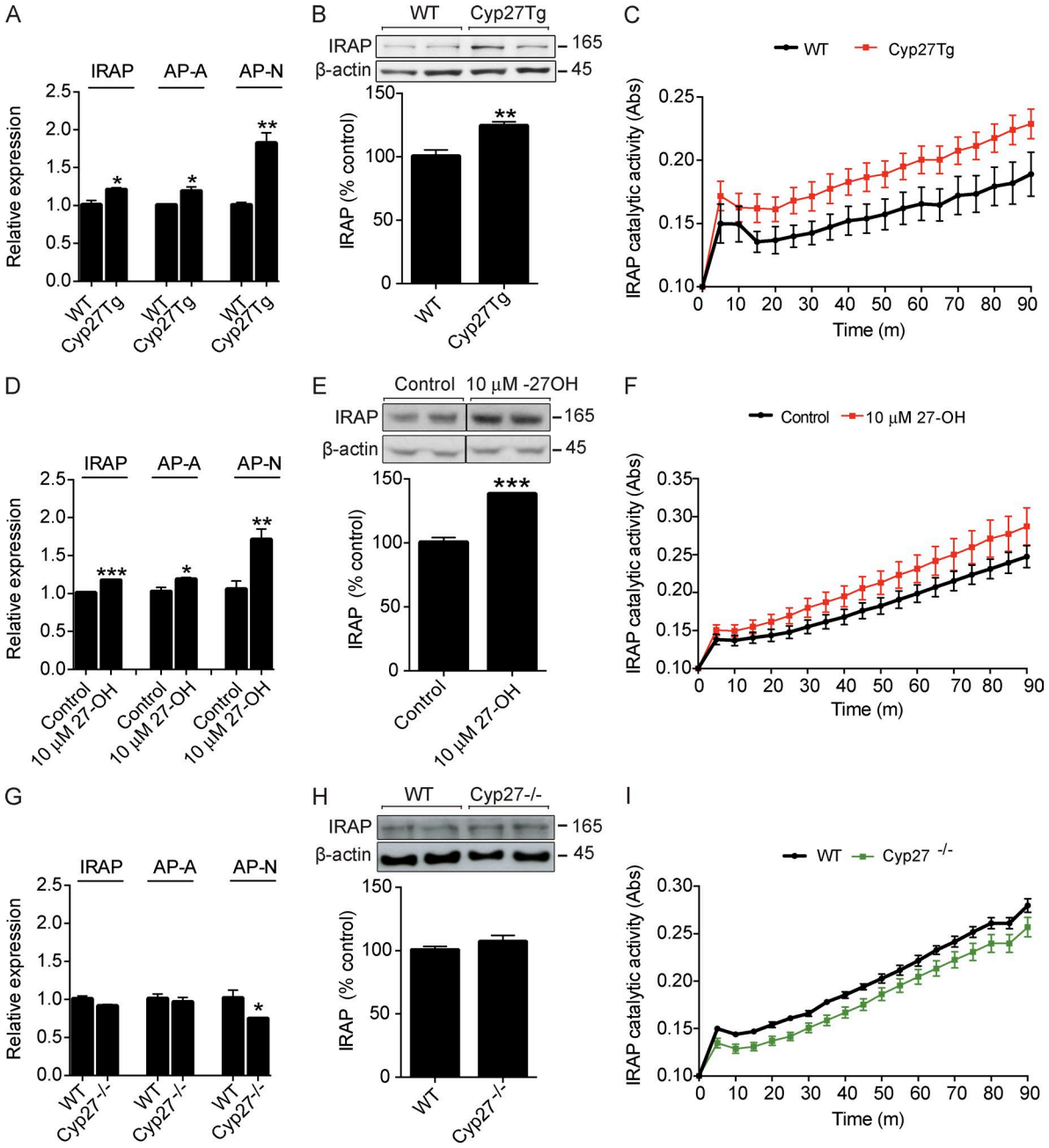

Figure 7. **AP-N and IRAP in *Cyp27a1* overexpression, ICV27-OH, and sterol 27-hydroxylase–deficient mice.** (A) Expression levels of IRAP, AP-A, and AP-N mRNA in Cyp27Tg mice compared with WT littermate mice. (B) Brain homogenates from WT and Cyp27Tg mice immunoblotted against IRAP. Histograms show normalized data as a ratio to actin levels and expressed as a percentage of WT mice ($n = 4$). (C) Membrane preparation extracts from WT and Cyp27Tg mice used to measure the IRAP catalytic activity ($n = 19$; $P < 0.0001$). (D) ICV injections of 10 µM 27-OH (ICV27-OH) and artificial CSF (control) in 7–8-wk-old C57BL/6 mice showing mRNA levels of IRAP, AP-A, and AP-N. (E and F) Protein levels of IRAP (E) and IRAP catalytic activity (F) from ICV27-OH and control mice ($n = 4$). (G) mRNA expression analyses of AP-N, IRAP, and AP-A in $Cyp27^{-/-}$ and WT mice ($n = 4$). (H) Brain homogenates from WT and $Cyp27^{-/-}$ mice immunoblotted with IRAP antibody. (B, E, and H) Molecular mass is indicated in kilodaltons. (I) IRAP catalytic activity was determined in membrane preparations from these animals ($n = 19$; $P < 0.0001$). Data are presented as mean ± SEM; *, $P < 0.05$; **, $P < 0.01$; ***, $P < 0.001$. An unpaired Student's two-tailed *t* tests was used for all comparisons except IRAP catalytic activity, where a paired Student's *t* test was used. The indicated sample size was obtained from at least two experiments.

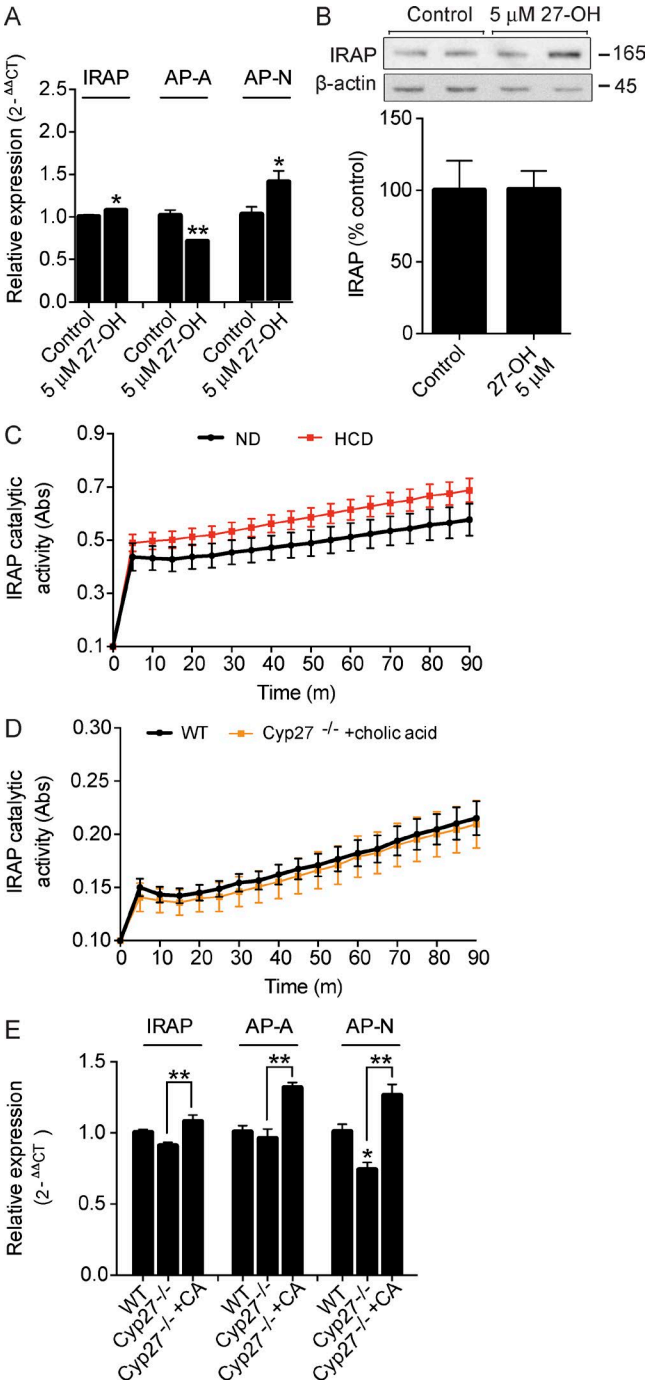

Figure 8. **IRAP expression and catalytic activity in different in vivo mouse models.** (A) ICV injections of 5 µM of 27-OH (ICV27-OH) and artificial CSF (control) mice showing mRNA levels of IRAP, AP-A, and AP-N (n = 4). (B) IRAP protein levels from ICV27-OH and control mice (n = 4). Molecular mass is indicated in kilodaltons. (C) IRAP catalytic activity in membrane preparations from WT (C57BL/6) mice fed a normal diet or an HCD (n = 19; $P < 0.0001$). (D) IRAP catalytic activity in membrane preparations from cerebral extracts of Cyp27$^{-/-}$ mice treated with 0.5% CA. (E) IRAP, AP-A, and AP-N mRNA levels from the brain of these animals are shown (n = 4). Data are presented as mean ± SEM; *, $P < 0.05$; **, $P < 0.01$. An unpaired Student's two-tailed t test was used for all comparisons except IRAP catalytic activity, where a paired Student's t test was used. ND, normal diet; Cyp27$^{-/-}$, CYP27a1 knockout mice. The indicated sample size was obtained from at least two experiments.

RNA extraction and real-time RT-PCR

Total RNA extraction and reverse transcription and real-time PCR amplification assays were performed as previously reported (Mateos et al., 2011b). Three biological replicates per group were analyzed for each gene, and the gene expression value was calculated as the mean of three independent measurements. The relative quantification of all targets was performed using the comparative cycle threshold method, $2^{-\Delta\Delta Ct}$, where $\Delta\Delta Ct = (Ct_{\text{target gene}} - Ct_{\text{GAPDH}})_{\text{treated}} - (Ct_{\text{target gene}} - Ct_{\text{GAPDH}})_{\text{untreated}}$. The mean was obtained after the $2^{-\Delta\Delta Ct}$ calculation of cDNA for each sample in triplicate, and the relative transcription levels are expressed as mean ± SEM.

Preparation of membrane proteins

Before harvesting, confluent cells grown in 5% CO_2 at 37°C were washed with PBS and then briefly treated with PBS, pH 7.4, containing 0.2% EDTA (wt/vol). The cell suspension was centrifuged for 5 min at 500 g at room temperature and resuspended in PBS, after which the number of cells was counted. After one more wash step, cells were homogenized in 50 mM Tris-HCl, pH 7.4, using a Potter homogenizer (30 strokes at 1,000 rpm). Homogenates were centrifuged at 760 g for 5 min to remove nuclei and unbroken cells. The supernatant was centrifuged for 30 min (30,000 g at 4°C). The supernatant was removed, and the resulting cell membrane–containing pellets were stored at −20°C until use.

Catalytic activity of IRAP

Determination of the cystinyl aminopeptidase catalytic activity is based on the cleavage of the substrate L-leucine-p-nitroanilide (L-Leu-pNA) into L-leucine and p-nitroaniline (Demaegdt et al., 2004). This latter compound displays a characteristic light absorption maximum at 405 nm. Cell membrane–containing pellets (described in the Preparation of membrane proteins section) were resuspended using an enzyme buffer containing 50 mM Tris-HCl, pH 7.4, 140 mM NaCl, 0.1% (wt/vol) BSA, and 100 µM PMSF. The incubation mixture comprised 50 µl membrane homogenate (at a concentration corresponding to 50 µg proteins) and 1.5 mM 200 µl L-Leu-pNA. Membrane homogenate mixtures were incubated at 37°C in 96-well plates, and the formation of p-nitroaniline was measured by absorption at 405 nm between 5 and 90 min in a microplate reader. Enzymatic activity was calculated by absorbance analysis at sequential time points.

LXRβ, AP-N, and AP-A knockdown by siRNA transfection

Rat primary cultures (80% confluence) were transfected with LXRβ siRNA, AP-N siRNA, or AP-A siRNA to a final concentration of 25 nM per well and using 4 µl DharmaFECT 3 reagent (GE Healthcare and Thermo Fisher Scientific) ac-

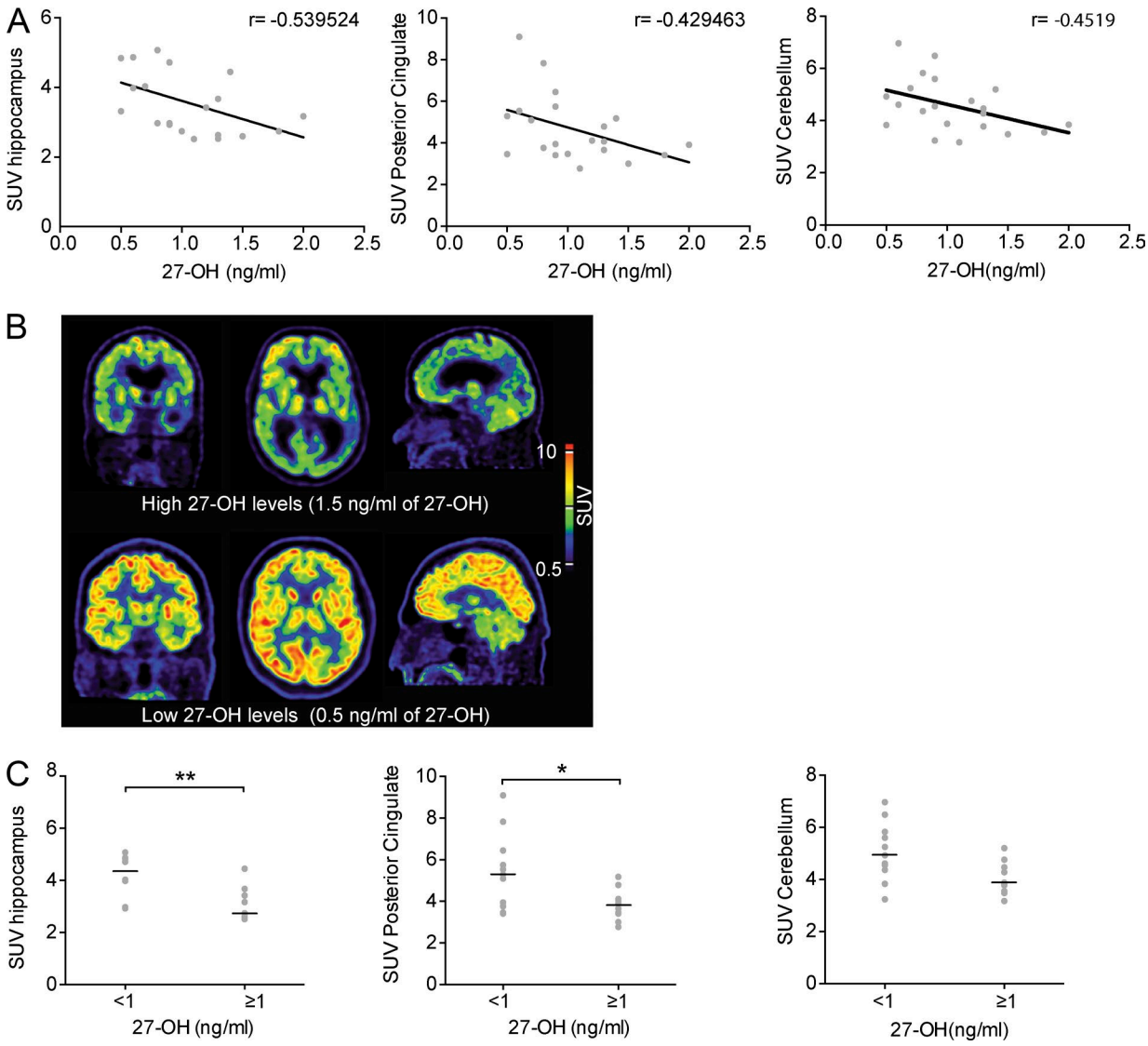

Figure 9. **Association of CSF 27-OH levels and brain glucose metabolism deficits in humans.** (A) Correlation between ^{18}F-FDG uptake (SUV) and CSF 27-OH levels in the hippocampus (left, $r = -0.539$, P = 0.011), posterior cingulate (middle, $r = -0.429$, P = 0.05), and cerebellum (right, $r = -0,4519$, P = 0.04) of patients, by Spearman rank correlation. (B) Representative brain ^{18}F-FDG PET/MRI images from a patient with higher (1.5 ng/ml) and lower (0.5 ng/ml) 27-OH levels in the CSF (top and bottom, respectively). (C) Quantification of SUV in the hippocampus (left), posterior cingulate (middle), and cerebellum (right) of patients with <1 ng/ml and ≥1 ng/ml 27-OH. Lines indicate median values. *, P < 0.05; **, P < 0.01 by Mann–Whitney *U* test.

cording to the manufacturer's instructions. The siRNAs for LXRβ (ON-TARGET plus SMARTpool, L-088852-01-0020), AP-N (ON-TARGET plus SMARTpool, L-08084-02-0020), and AP-A (ON-TARGET plus SMARTpool, L-098194-02-0020) were designed by and acquired from GE Healthcare. Knockdown efficiency was monitored at the mRNA level by real-time RT-PCR.

Determination of glucose uptake

Rat primary neurons were seeded in 96-well plates and maintained as previously described (Mateos et al., 2009). However, rat primary neurons were substituted for *SH-SY5Y* cells, as similar results were found in both cell types (Figs. 3 A and 5 C). This is in accordance with the replacement requirement of the guiding principles of ethical use of animals 3Rs (replacement, reduction, and refinement). *SH-SY5Y* cells were grown in 24-well plates with MEM supplemented with 10% FBS until 80% confluence. Treatments were with 1 µM 27-OH (24 h) and 10 µM bestatin (24 h); however, when 1 µM AngIV and 1 µM AngIII (Bachem) were added, this was done in the last 3 h of the 27-OH treatment. Insulin was used at 100 nM. For the combination of 27-OH and insulin, 1 µM 27-OH was applied for 24 h, followed by insulin for 3 h. A fluorescent glucose analogue, 2-NBDG (Invitrogen),

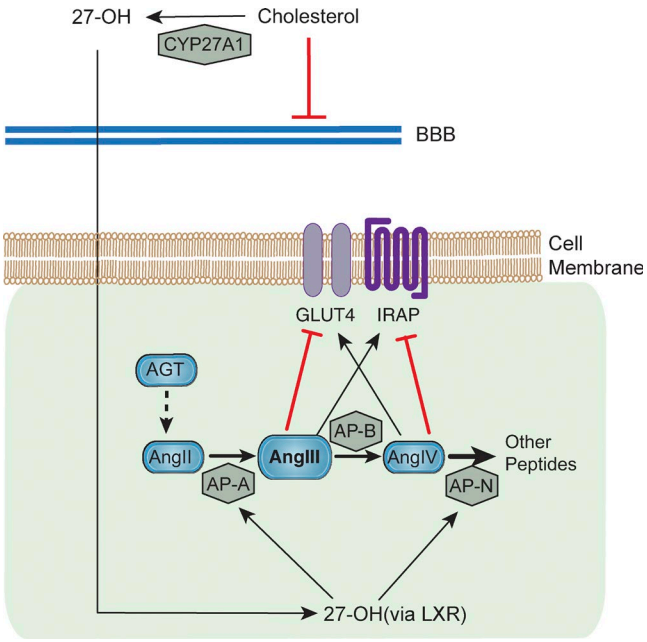

Figure 10. **Schematic overview of the mechanism by which 27-OH decreases brain glucose uptake 27-OH increases the expression of AP-A and AP-N via LXR.** An increase in AP-A results in higher production of AngIII, whereas higher AP-N would enhance degradation of AngIV and thus alter the balance between AngIII, an IRAP activator and glucose uptake inhibitor, and AngIV, an IRAP inhibitor and glucose uptake activator. AGT, angiotensinogen; Ang, angiotensin; AP, aminopeptidase.

was used at 100 µM diluted in HBSS (Sigma-Aldrich). After incubation at 37°C for 1 h with the analogue in addition to the treatments, culture medium was removed and fluorescence was measured (after repeated washing and addition of PBS) in a fluorescence microplate reader, set at an excitation wavelength of 466 nm and an emission wavelength of 540 nm. Experimental outcomes are indicated as a percent reduction of fluorimetric response with respect to controls. Results are expressed as means ± SEM.

Immunofluorescence

Primary neurons were seeded in low confluence (20%) on coverslips coated with poly-D-lysine (P6407; Sigma-Aldrich). After the indicated treatments, cells were prefixed with 2% paraformaldehyde for 2 min, fixed with 4% paraformaldehyde for 20 min, and washed with PBS. Blocking at room temperature for 30 min with 0.1 M PBS, pH 7.4, + 0.1% Triton + 1% BSA (Sigma-Aldrich) followed by an overnight 4°C incubation with the anti-IRAP antibody (1:50, 3808; Cell Signaling Technology) primary antibody. The secondary antibody, Alexa Fluor 546 donkey anti–rabbit IgG (A11035; Invitrogen), was incubated at room temperature for 30 min at a dilution of 1:1,000. Washing with PBS was done thoroughly between the different steps. The omission of the primary antibody was the control staining. Coverslips were mounted onto glass slides using ProLong Gold Antifade Reagent (Invitrogen). A ZEISS (LSM 510 META) confocal laser scanning system was used to obtain images. Image stacks consisting of 5–12 image planes were acquired (resolution, 1,024 × 1,024 and z step 0.5 µm) with 100× oil immersion (NA, 1.45).

Animal ^{18}F-FDG PET imaging

12-mo-old Cyp27Tg and WT mice were anesthetized by inhalation of 4–5% isoflurane in 100% oxygen. After induction of anesthesia, the isoflurane concentration was lowered to 1.5–2% in a 50:50 air/oxygen mixture, and a cannula was inserted into the tail vein for the ^{18}F-FDG tracer injection. Animals were under anesthesia for 30 min. After injection, withdrawn from anesthesia, the mice regained consciousness and were free to move for 45 min in a heated cage. The short anesthesia enables fast recovery of the animals. This procedure is important for an optimal ^{18}F-FDG uptake. Thereafter, anesthesia was reintroduced preceding the 40-min PET scan.

The nanoScan PET/MRI (Mediso Ltd.) was used in the study, exhibiting a 700-µm PET and 100-µm MRI in-plane spatial resolution. PET scans of 40-min list mode data were reconstructed into one time frame and corrected for random coincidences, attenuation, and scatter. The image reconstruction protocol consisted of a 400–600-keV energy window with a 5-ns time window, using a 20-iteration maximum-likelihood expectation maximization algorithm and a 10^{-4} regularization parameter, leading to a final isotropic resolution of 0.3 × 0.3 × 0.3 mm voxel size. Details on the reconstruction method have been previously published by us and others (Szanda et al., 2011; Nagy et al., 2013).

MRI images, in addition to being sequentially acquired after the PET scans, were spatially transformed to match the reconstructed PET images. The parameters used for the MRI scan were FSE 3D mouse (20-min scan), with 2,000/80 ms (TR/TE, respectively) and 130/130 frequency/phase. The magnitude of brain ^{18}F-FDG uptake was expressed as a percentage of SUV (%SUV). Computed as the concentration of ^{18}F-FDG in each region of interest (kBq/ml) divided by the injected dose (MBq) times the body weight of each animal (Kg). Individual data for each mouse can be found in Table S1. All reconstructed images were analyzed using PMOD Software (PMOD Technologies), and the power analysis was done with G*Power (3.1.7). PET experiments were conducted following approval from the local ethical committee of Karolinska Institutet, Stockholm.

Although PET is a well-established method to measure brain glucose uptake, it also has some limitations. Isoflurane anesthesia has a suppressive effect on neural activity that could have confounded our results. Some experiments have shown that brain glucose levels are significantly increased by isoflurane (Kofke et al., 1987). Another effect of isoflurane anesthesia is that it makes the glucose metabolic rate more uniform across the brain (Toyama et al., 2004); this limitation is suggested to be similar for both groups under investigation, WT and Cyp27Tg animals. In both our ^{18}F-FDG PET images in WT and Cyp27Tg animals, extracerebral regions

such as facial glands (including salivary, lacrimal, and Harderian) showed high ^{18}F-FDG uptake, consistent with previous studies by other groups (Mirrione et al., 2007; Zimmer et al., 2014). The potential spillover from those facial glands into our brain regions selected for PET quantification is expected to be negligible, especially when quantifying large regions including the cortex (149 mm^3), hippocampus (26 mm^3), and other regions, as well as when quantifying the uptake in the whole mouse brain.

For the quantification of ^{18}F-FDG uptake in mice, we have chosen to express ^{18}F-FDG uptake in SUVs. This is a widely used and a well-validated method both in small-animal PET (for review see Zimmer et al. [2014]) and in humans. It has been reported that PET uptake expressed in SUV is potentially confounded by cerebral blood flow differences between different animals, and an excellent correspondence between SUV and the results from the full kinetic quantification has been clarified elsewhere (Schiffer et al., 2007). We have counteracted these limitations by addressing the research questions with variant techniques and models.

Behavioral studies

At 12 mo of age, mice were trained in the MWM task to locate a hidden escape platform in a circular pool. The apparatus used in this study has been previously described (Maioli et al., 2013). During the first two trials of habituation, the swimming speed of Cyp27Tg and WT mice was measured, and no differences in speed or sensory motor functions (determined by visual cue test) were found between groups (Fig. 1 C), thus excluding effects of motivational or sensory motor factors on learning and memory performance. Escape latency was then used for the evaluation of spatial learning of mice. Each mouse had four trials a day for seven consecutive days with an inter-trial interval of 30 min (acquisition). Mice were released facing the pool wall from one of the starting points (north, east, south, northwest, or southeast) and allowed to search for the platform for up to 60 s. The position of the platform (southwest quadrant) remained unchanged among the acquisition days. For each trial, the starting position was changed and the sequence of starts were designed as such that the platform will be to the right or left of an animal during an equal number of trials (Vorhees and Williams, 2006). If a mouse did not find the platform, it was gently guided to it and allowed to remain there for 15 s. Memory retention was assessed on the eighth day during the probe test, in which the platform was removed. A single starting point (northeast) was used for all the mice. As measures of memory retention we used: the time of first occurrence to the position where the platform was located during acquisition (escape latency), the number of times that the mice crossed the former platform area (frequency on platform), and the time spent in the target quadrant of the platform (duration in platform sector). A video camera was placed above the center of the pool and connected to a video-tracking system (Ethovision XT 8; Noldus Information Technology).

Stereotaxic injections

After being anesthetized with an isoflurane/oxygen mixture, 7–8-wk-old C57BL/6 mice were placed on a stereotaxic frame (David Kopf Instruments) on a heated pad at 37°C to maintain normal body temperature. 27-OH was associated with HDL (ab77881; Abcam) at a concentration ratio of 1:3 and incubated together at 37°C for 1 h and diluted in artificial CSF (3525; R&D Systems) to concentrations of 10 or 5 µM. Bilateral injections into the lateral ventricle using a 10-µl-gauge Hamilton syringe were performed. 1 µl of solution containing 10 or 5 µM 27-OH loaded HDL at was injected per hemisphere. Control group was injected under the same conditions with HDL diluted in artificial CSF. The injection site coordinates were −0.9 mm anteroposterior, ±1.4 mm lateral from the bregma, and 2.0 mm from the skull surface according to Paxinos mouse brain atlas (Paxinos and Franklin, 2001). Ethical consent was received from the regional ethical committee for animal studies.

Determination of 27-OH and CA

Quantification of 27-OH levels from the obtained CSF of the above-selected patients was done using isotope dilution mass spectrometry as described previously (Dzeletovic et al., 1995). The same method was also used for the quantification of brain CA with the use of deuterium-labeled CA as an internal standard.

Statistical analysis

Results are expressed as mean ± SEM except where otherwise stated. Statistical differences from experimental studies were analyzed by unpaired Student's *t* test, except in the behavioral studies, where a repeated-measures ANOVA (acquisition phase) and Mann–Whitney *U* test (probe test) were used, and studies including human data, where Spearman rank correlation coefficients and Mann–Whitney *U* tests were applied. Experiments including IRAP catalytic activity were analyzed by paired Student's *t* test. Values of $P < 0.05$ were considered statistically significant in all analyses.

Online supplemental material

Table S1 shows injected doses and weights of mice. Table S2 lists the demographic data of the included patients.

ACKNOWLEDGMENTS

We would like to thank Olga Voevodskaya, Seyed-Mohammad Fereshtehnejad, and Soheil Damangir for assisting with statistical analyses and Miklós Tóth (Karolinska Experimental Research and Imaging Centre) and Elena Rodriguez-Vieitez for their

help with the micro-PET studies. We also share our appreciation with the patients taking part in the study.

This research was supported by the following Swedish foundations: Swedish Brain Power, the regional agreement on medical training and clinical research (ALF) between the Stockholm County Council and Karolinska Institutet, the Strategic Neuroscience Program, the Margaretha af Ugglas Foundation, Stiftelse Olle Engkvist Byggmästare, Gun och Bertil Stohnes Stiftelse, the Karolinska Institutet fund for geriatric research, Stiftelsen Gamla Tjänarinnor, Hjärnfonden, and Alzheimerfonden.

The authors declare no competing financial interests.

Author contributions: Conceptualization, A. Cedazo-Mínguez and I. Björkhem; Methodology, A. Cedazo-Mínguez, I. Björkhem, M.-A.-M. Ismail, and L. Mateos; Investigation, M.-A.-M. Ismail, L. Mateos, S. Maioli, P. Merino-Serrais, and M. Lodeiro; Resources, E. Leitersdorf, Z. Ali, E. Westman, L. Olof-Wahlund, and I. Savitcheva; Formal analysis, M.-A.-M. Ismail, L. Mateos, and S. Maioli; Writing–original draft, M.-A.-M. Ismail, L. Mateos, and A. Cedazo-Mínguez; Writing–review and editing, all authors; Funding acquisition, A. Cedazo-Mínguez, I. Björkhem, and M.-A.-M. Ismail; Supervision, B. Winblad, I. Björkhem, and A. Cedazo-Mínguez.

Submitted: 14 April 2016
Revised: 17 August 2016
Accepted: 28 October 2016

REFERENCES

Abhold, R.H., M.J. Sullivan, J.W. Wright, and J.W. Harding. 1987. Binding, degradation and pressor activity of angiotensins II and III after aminopeptidase inhibition with amastatin and bestatin. *J. Pharmacol. Exp. Ther.* 242:957–962.

Albiston, A.L., S.G. McDowall, D. Matsacos, P. Sim, E. Clune, T. Mustafa, J. Lee, F.A. Mendelsohn, R.J. Simpson, L.M. Connolly, and S.Y. Chai. 2001. Evidence that the angiotensin IV (AT_4) receptor is the enzyme insulin-regulated aminopeptidase. *J. Biol. Chem.* 276:48623–48626. http://dx.doi.org/10.1074/jbc.C100512200

Albiston, A.L., C.J. Morton, H.L. Ng, V. Pham, H.R. Yeatman, S. Ye, R.N. Fernando, D. De Bundel, D.B. Ascher, F.A.O. Mendelsohn, et al. 2008. Identification and characterization of a new cognitive enhancer based on inhibition of insulin-regulated aminopeptidase. *FASEB J.* 22:4209–4217. http://dx.doi.org/10.1096/fj.08-112227

Apelt, J., G. Mehlhorn, and R. Schliebs. 1999. Insulin-sensitive GLUT4 glucose transporters are colocalized with GLUT3-expressing cells and demonstrate a chemically distinct neuron-specific localization in rat brain. *J. Neurosci. Res.* 57:693–705. http://dx.doi.org/10.1002/(SICI)1097-4547(19990901)57:5<693::AID-JNR11>3.0.CO;2-X

Attwell, D., and S.B. Laughlin. 2001. An energy budget for signaling in the grey matter of the brain. *J. Cereb. Blood Flow Metab.* 21:1133–1145. http://dx.doi.org/10.1097/00004647-200110000-00001

Båvner, A., M. Shafaati, M. Hansson, M. Olin, S. Shpitzen, V. Meiner, E. Leitersdorf, and I. Björkhem. 2010. On the mechanism of accumulation of cholestanol in the brain of mice with a disruption of sterol 27-hydroxylase. *J. Lipid Res.* 51:2722–2730. http://dx.doi.org/10.1194/jlr.M008326

Björkhem, I., M. Heverin, V. Leoni, S. Meaney, and U. Diczfalusy. 2006. Oxysterols and Alzheimer's disease. *Acta Neurol. Scand. Suppl.* 114:43–49. http://dx.doi.org/10.1111/j.1600-0404.2006.00684.x

Björkhem, I., A. Cedazo-Minguez, V. Leoni, and S. Meaney. 2009. Oxysterols and neurodegenerative diseases. *Mol. Aspects Med.* 30:171–179. http://dx.doi.org/10.1016/j.mam.2009.02.001

Brant, A.M., T.J. Jess, G. Milligan, C.M. Brown, and G.W. Gould. 1993. Immunological analysis of glucose transporters expressed in different regions of the rat brain and central nervous system. *Biochem. Biophys. Res. Commun.* 192:1297–1302. http://dx.doi.org/10.1006/bbrc.1993.1557

Burgos-Ramos, E., A. Hervás-Aguilar, D. Aguado-Llera, L. Puebla-Jiménez, A.M. Hernández-Pinto, V. Barrios, and E. Arilla-Ferreiro. 2008. Somatostatin and Alzheimer's disease. *Mol. Cell. Endocrinol.* 286:104–111. http://dx.doi.org/10.1016/j.mce.2008.01.014

De Bundel, D., I. Smolders, R. Yang, A.L. Albiston, Y. Michotte, and S.Y. Chai. 2009. Angiotensin IV and LVV-haemorphin 7 enhance spatial working memory in rats: effects on hippocampal glucose levels and blood flow. *Neurobiol. Learn. Mem.* 92:19–26. http://dx.doi.org/10.1016/j.nlm.2009.02.004

De Bundel, D., H. Demaegdt, T. Lahoutte, V. Caveliers, K. Kersemans, A.G. Ceulemans, G. Vauquelin, R. Clinckers, P. Vanderheyden, Y. Michotte, and I. Smolders. 2010. Involvement of the AT1 receptor subtype in the effects of angiotensin IV and LVV-haemorphin 7 on hippocampal neurotransmitter levels and spatial working memory. *J. Neurochem.* 112:1223–1234. http://dx.doi.org/10.1111/j.1471-4159.2009.06547.x

Demaegdt, H., P. Vanderheyden, J.P. De Backer, S. Mosselmans, H. Laeremans, M.T. Le, V. Kersemans, Y. Michotte, and G. Vauquelin. 2004. Endogenous cystinyl aminopeptidase in Chinese hamster ovary cells: characterization by [125I]Ang IV binding and catalytic activity. *Biochem. Pharmacol.* 68:885–892. http://dx.doi.org/10.1016/j.bcp.2004.05.047

Dzeletovic, S., O. Breuer, E. Lund, and U. Diczfalusy. 1995. Determination of cholesterol oxidation products in human plasma by isotope dilution-mass spectrometry. *Anal. Biochem.* 225:73–80. http://dx.doi.org/10.1006/abio.1995.1110

El Messari, S., C. Leloup, M. Quignon, M.-J. Brisorgueil, L. Penicaud, and M. Arluison. 1998. Immunocytochemical localization of the insulin-responsive glucose transporter 4 (Glut4) in the rat central nervous system. *J. Comp. Neurol.* 399:492–512. http://dx.doi.org/10.1002/(SICI)1096-9861(19981005)399:4<492::AID-CNE4>3.0.CO;2-X

El Messari, S., A. Aït-Ikhlef, D.H. Ambroise, L. Penicaud, and M. Arluison. 2002. Expression of insulin-responsive glucose transporter GLUT4 mRNA in the rat brain and spinal cord: an in situ hybridization study. *J. Chem. Neuroanat.* 24:225–242. http://dx.doi.org/10.1016/S0891-0618(02)00058-3

Fernando, R.N., A.L. Albiston, and S.Y. Chai. 2008. The insulin-regulated aminopeptidase IRAP is colocalised with GLUT4 in the mouse hippocampus - potential role in modulation of glucose uptake in neurones? *Eur. J. Neurosci.* 28:588–598. http://dx.doi.org/10.1111/j.1460-9568.2008.06347.x

Funaki, M., P. Randhawa, and P.A. Janmey. 2004. Separation of insulin signaling into distinct GLUT4 translocation and activation steps. *Mol. Cell. Biol.* 24:7567–7577. http://dx.doi.org/10.1128/MCB.24.17.7567-7577.2004

Gao, J., Y. Marc, X. Iturrioz, V. Leroux, F. Balavoine, and C. Llorens-Cortes. 2014. A new strategy for treating hypertension by blocking the activity of the brain renin-angiotensin system with aminopeptidase A inhibitors. *Clin. Sci.* 127:135–148. http://dx.doi.org/10.1042/CS20130396

Goldstein, F.C., A.V. Ashley, Y.W. Endeshaw, J. Hanfelt, J.J. Lah, and A.I. Levey. 2008. Effects of hypertension and hypercholesterolemia on cognitive functioning in patients with Alzheimer disease. *Alzheimer Dis. Assoc. Disord.* 22:336–342. http://dx.doi.org/10.1097/WAD.0b013e318188e80d

Heverin, M., N. Bogdanovic, D. Lütjohann, T. Bayer, I. Pikuleva, L. Bretillon, U. Diczfalusy, B. Winblad, and I. Björkhem. 2004. Changes in the levels of cerebral and extracerebral sterols in the brain of patients with Alzheimer's disease. *J. Lipid Res.* 45:186–193. http://dx.doi.org/10.1194/jlr.M300320-JLR200

Hottman, D.A., D. Chernick, S. Cheng, Z. Wang, and L. Li. 2014. HDL and cognition in neurodegenerative disorders. *Neurobiol. Dis.* 72:22–36. http://dx.doi.org/10.1016/j.nbd.2014.07.015

Kivipelto, M., E.L. Helkala, M.P. Laakso, T. Hänninen, M. Hallikainen, K. Alhainen, H. Soininen, J. Tuomilehto, and A. Nissinen. 2001. Midlife vascular risk factors and Alzheimer's disease in later life: Longitudinal, population based study. *BMJ.* 322:1447–1451. http://dx.doi.org/10.1136/bmj.322.7300.1447

Knight, E.M., I.V.A. Martins, S. Gümüsgöz, S.M. Allan, and C.B. Lawrence. 2014. High-fat diet-induced memory impairment in triple-transgenic Alzheimer's disease (3xTgAD) mice is independent of changes in amyloid and tau pathology. *Neurobiol. Aging.* 35:1821–1832. http://dx.doi.org/10.1016/j.neurobiolaging.2014.02.010

Kofke, W.A., R.A. Hawkins, D.W. Davis, and J.F. Biebuyck. 1987. Comparison of the effects of volatile anesthetics on brain glucose metabolism in rats. *Anesthesiology.* 66:810–813. http://dx.doi.org/10.1097/00000542-198706000-00016

Leloup, C., M. Arluison, N. Kassis, N. Lepetit, N. Cartier, P. Ferré, and L. Pénicaud. 1996. Discrete brain areas express the insulin-responsive glucose transporter GLUT4. *Brain Res. Mol. Brain Res.* 38:45–53. http://dx.doi.org/10.1016/0169-328X(95)00306-D

Leoni, V., and C. Caccia. 2011. Oxysterols as biomarkers in neurodegenerative diseases. *Chem. Phys. Lipids.* 164:515–524. http://dx.doi.org/10.1016/j.chemphyslip.2011.04.002

Leto, D., and A.R. Saltiel. 2012. Regulation of glucose transport by insulin: Traffic control of GLUT4. *Nat. Rev. Mol. Cell Biol.* 13:383–396. http://dx.doi.org/10.1038/nrm3351

Lew, R.A., T. Mustafa, S. Ye, S.G. McDowall, S.Y. Chai, and A.L. Albiston. 2003. Angiotensin AT4 ligands are potent, competitive inhibitors of insulin regulated aminopeptidase (IRAP). *J. Neurochem.* 86:344–350. http://dx.doi.org/10.1046/j.1471-4159.2003.01852.x

Luan, Y., and W. Xu. 2007. The structure and main functions of aminopeptidase N. *Curr. Med. Chem.* 14:639–647. http://dx.doi.org/10.2174/092986707780059571

Maioli, S., A. Båvner, Z. Ali, M. Heverin, M.A. Ismail, E. Puerta, M. Olin, A. Saeed, M. Shafaati, P. Parini, et al. 2013. Is it possible to improve memory function by upregulation of the cholesterol 24S-hydroxylase (CYP46A1) in the brain? *PLoS One.* 8:e68534. http://dx.doi.org/10.1371/journal.pone.0068534

Mateos, L., S. Akterin, F.J. Gil-Bea, S. Spulber, A. Rahman, I. Björkhem, M. Schultzberg, A. Flores-Morales, and A. Cedazo-Mínguez. 2009. Activity-regulated cytoskeleton-associated protein in rodent brain is down-regulated by high fat diet in vivo and by 27-hydroxycholesterol in vitro. *Brain Pathol.* 19:69–80. http://dx.doi.org/10.1111/j.1750-3639.2008.00174.x

Mateos, L., M.A. Ismail, F.J. Gil-Bea, V. Leoni, B. Winblad, I. Björkhem, and A. Cedazo-Mínguez. 2011a. Upregulation of brain renin angiotensin system by 27-hydroxycholesterol in Alzheimer's disease. *J. Alzheimers Dis.* 24:669–679. http://dx.doi.org/10.3233/JAD-2011-101512

Mateos, L., M.A. Ismail, F.J. Gil-Bea, R. Schüle, L. Schöls, M. Heverin, R. Folkesson, I. Björkhem, and A. Cedazo-Mínguez. 2011b. Side chain-oxidized oxysterols regulate the brain renin-angiotensin system through a liver X receptor-dependent mechanism. *J. Biol. Chem.* 286:25574–25585. http://dx.doi.org/10.1074/jbc.M111.236877

Mazurek, M.F., J.H. Growdon, M.F. Beal, and J.B. Martin. 1986. CSF vasopressin concentration is reduced in Alzheimer's disease. *Neurology.* 36:1133–1137. http://dx.doi.org/10.1212/WNL.36.8.1133

McEwen, B.S., and L.P. Reagan. 2004. Glucose transporter expression in the central nervous system: Relationship to synaptic function. *Eur. J. Pharmacol.* 490:13–24. http://dx.doi.org/10.1016/j.ejphar.2004.02.041

McNay, E.C., R.C. McCarty, and P.E. Gold. 2001. Fluctuations in brain glucose concentration during behavioral testing: dissociations between brain areas and between brain and blood. *Neurobiol. Learn. Mem.* 75:325–337. http://dx.doi.org/10.1006/nlme.2000.3976

Meir, K., D. Kitsberg, I. Alkalay, F. Szafer, H. Rosen, S. Shpitzen, L.B. Avi, B. Staels, C. Fievet, V. Meiner, et al. 2002. Human sterol 27-hydroxylase (CYP27) overexpressor transgenic mouse model. Evidence against 27-hydroxycholesterol as a critical regulator of cholesterol homeostasis. *J. Biol. Chem.* 277:34036–34041. http://dx.doi.org/10.1074/jbc.M201122200

Mirrione, M.M., W.K. Schiffer, J.S. Fowler, D.L. Alexoff, S.L. Dewey, and S.E. Tsirka. 2007. A novel approach for imaging brain-behavior relationships in mice reveals unexpected metabolic patterns during seizures in the absence of tissue plasminogen activator. *Neuroimage.* 38:34–42. http://dx.doi.org/10.1016/j.neuroimage.2007.06.032

Nagy, K., M. Tóth, P. Major, G. Patay, G. Egri, J. Häggkvist, A. Varrone, L. Farde, C. Halldin, and B. Gulyás. 2013. Performance evaluation of the small-animal nanoScan PET/MRI system. *J. Nucl. Med.* 54:1825–1832. http://dx.doi.org/10.2967/jnumed.112.119065

Nordberg, A., J.O. Rinne, A. Kadir, and B. Långström. 2010. The use of PET in Alzheimer disease. *Nat. Rev. Neurol.* 6:78–87. http://dx.doi.org/10.1038/nrneurol.2009.217

Pancani, T., K.L. Anderson, L.D. Brewer, I. Kadish, C. DeMoll, P.W. Landfield, E.M. Blalock, N.M. Porter, and O. Thibault. 2013. Effect of high-fat diet on metabolic indices, cognition, and neuronal physiology in aging F344 rats. *Neurobiol. Aging.* 34:1977–1987. http://dx.doi.org/10.1016/j.neurobiolaging.2013.02.019

Paxinos, G., and K.B.J. Franklin. 2001. The Mouse Brain in Stereotaxic Coordinates. Second edition. Academic Press, San Diego, CA. 296 pp.

Pettersson, A.M.L., B.M. Stenson, S. Lorente-Cebrián, D.P. Andersson, N. Mejhert, J. Krätzel, G. Aström, I. Dahlman, A.V. Chibalin, P. Arner, and J. Laurencikiene. 2013. LXR is a negative regulator of glucose uptake in human adipocytes. *Diabetologia.* 56:2044–2054. http://dx.doi.org/10.1007/s00125-013-2954-5

Reiman, E.M., K. Chen, J.B. Langbaum, W. Lee, C. Reschke, D. Bandy, G.E. Alexander, and R.J. Caselli. 2010. Higher serum total cholesterol levels in late middle age are associated with glucose hypometabolism in brain regions affected by Alzheimer's disease and normal aging. *Neuroimage.* 49:169–176. http://dx.doi.org/10.1016/j.neuroimage.2009.07.025

Rossor, M.N., L.L. Iversen, C.Q. Mountjoy, M. Roth, J. Hawthorn, V.Y. Ang, and J.S. Jenkins. 1980. Arginine vasopressin and choline acetyltransferase in brains of patients with Alzheimer type senile dementia. *Lancet.* 316:1367–1368. http://dx.doi.org/10.1016/S0140-6736(80)92428-9

Saveanu, L., and P. van Endert. 2012. The role of insulin-regulated aminopeptidase in MHC class I antigen presentation. *Front. Immunol.* 3:57. http://dx.doi.org/10.3389/fimmu.2012.00057

Schiffer, W.K., M.M. Mirrione, and S.L. Dewey. 2007. Optimizing experimental protocols for quantitative behavioral imaging with 18F-FDG in rodents. *J. Nucl. Med.* 48:277–287.

Simpson, I.A., A. Carruthers, and S.J. Vannucci. 2007. Supply and demand in cerebral energy metabolism: The role of nutrient transporters. *J. Cereb. Blood Flow Metab.* 27:1766–1791. http://dx.doi.org/10.1038/sj.jcbfm.9600521

Stragier, B., D. De Bundel, S. Sarre, I. Smolders, G. Vauquelin, A. Dupont, Y. Michotte, and P. Vanderheyden. 2008. Involvement of insulin-regulated aminopeptidase in the effects of the renin-angiotensin fragment angiotensin IV: A review. *Heart Fail. Rev.* 13:321–337. http://dx.doi.org/10.1007/s10741-007-9062-x

Szanda, I., J. Mackewn, G. Patay, P. Major, K. Sunassee, G.E. Mullen, G. Nemeth, Y. Haemisch, P.J. Blower, and P.K. Marsden. 2011. National Electrical Manufacturers Association NU-4 performance evaluation of the PET component of the NanoPET/CT preclinical PET/CT scanner. *J. Nucl. Med.* 52:1741–1747. http://dx.doi.org/10.2967/jnumed.111.088260

Teune, L.K., A.L. Bartels, B.M. de Jong, A.T. Willemsen, S.A. Eshuis, J.J. de Vries, J.C. van Oostrom, and K.L. Leenders. 2010. Typical cerebral metabolic patterns in neurodegenerative brain diseases. *Mov. Disord.* 25:2395–2404. http://dx.doi.org/10.1002/mds.23291

Theofilopoulos, S., Y. Wang, S.S. Kitambi, P. Sacchetti, K.M. Sousa, K. Bodin, J. Kirk, C. Saltó, M. Gustafsson, E.M. Toledo, et al. 2013. Brain endogenous liver X receptor ligands selectively promote midbrain neurogenesis. *Nat. Chem. Biol.* 9:126–133. http://dx.doi.org/10.1038/nchembio.1156

Toyama, H., M. Ichise, J.S. Liow, D.C. Vines, N.M. Seneca, K.J. Modell, J. Seidel, M.V. Green, and R.B. Innis. 2004. Evaluation of anesthesia effects on [^{18}F]FDG uptake in mouse brain and heart using small animal PET. *Nucl. Med. Biol.* 31:251–256. http://dx.doi.org/10.1016/S0969-8051(03)00124-0

Vanderheyden, P.M. 2009. From angiotensin IV binding site to AT4 receptor. *Mol. Cell. Endocrinol.* 302:159–166. http://dx.doi.org/10.1016/j.mce.2008.11.015

Vannucci, S.J., F. Maher, and I.A. Simpson. 1997. Glucose transporter proteins in brain: delivery of glucose to neurons and glia. *Glia.* 21:2–21. http://dx.doi.org/10.1002/(SICI)1098-1136(199709)21:1<2::AID-GLIA2>3.0.CO;2-C

Vannucci, S.J., E.M. Koehler-Stec, K. Li, T.H. Reynolds, R. Clark, and I.A. Simpson. 1998. GLUT4 glucose transporter expression in rodent brain: effect of diabetes. *Brain Res.* 797:1–11. http://dx.doi.org/10.1016/S0006-8993(98)00103-6

von Bohlen und Halbach, O., and D. Albrecht. 2006. The CNS renin-angiotensin system. *Cell Tissue Res.* 326:599–616. http://dx.doi.org/10.1007/s00441-006-0190-8

Vorhees, C.V., and M.T. Williams. 2006. Morris water maze: Procedures for assessing spatial and related forms of learning and memory. *Nat. Protoc.* 1:848–858. http://dx.doi.org/10.1038/nprot.2006.116

Wallis, M.G., M.F. Lankford, and S.R. Keller. 2007. Vasopressin is a physiological substrate for the insulin-regulated aminopeptidase IRAP. *Am. J. Physiol. Endocrinol. Metab.* 293:E1092–E1102. http://dx.doi.org/10.1152/ajpendo.00440.2007

Wirth, M., S. Villeneuve, C.M. Haase, C.M. Madison, H. Oh, S.M. Landau, G.D. Rabinovici, and W.J. Jagust. 2013. Associations between Alzheimer disease biomarkers, neurodegeneration, and cognition in cognitively normal older people. *JAMA Neurol.* 70:1512–1519. http://dx.doi.org/10.1001/jamaneurol.2013.4013

World Health Organization. 1992. The ICD-10 Classification of Mental and Behavioural Disorders: Clinical Descriptions and Diagnostic Guidelines. World Health Organization, Geneva, Switzerland. 362 pp.

Wright, J.W., and J.W. Harding. 2008. The angiotensin AT4 receptor subtype as a target for the treatment of memory dysfunction associated with Alzheimer's disease. *J. Renin Angiotensin Aldosterone Syst.* 9:226–237. http://dx.doi.org/10.1177/1470320308099084

Yugandhar, V.G., and M.A. Clark. 2013. Angiotensin III: A physiological relevant peptide of the renin angiotensin system. *Peptides.* 46:26–32. http://dx.doi.org/10.1016/j.peptides.2013.04.014

Zimmer, E.R., M.J. Parent, A.C. Cuello, S. Gauthier, and P. Rosa-Neto. 2014. MicroPET imaging and transgenic models: A blueprint for Alzheimer's disease clinical research. *Trends Neurosci.* 37:629–641. http://dx.doi.org/10.1016/j.tins.2014.07.002